Analytical solutions to statistical moments for transient flow in two-dimensional, bounded, randomly heterogeneous media

Zhiming Lu

Hydrology, Geochemistry, and Geology Group, Los Alamos National Laboratory, Los Alamos, New Mexico, USA

Dongxiao Zhang

Mewbourne School of Petroleum and Geological Engineering, University of Oklahoma, Norman, Oklahoma, USA

Received 3 June 2004; revised 15 October 2004; accepted 4 November 2004; published 27 January 2005.

[1] In this paper we derive analytical solutions to statistical moments for transient saturated flow in two-dimensional, bounded, randomly heterogeneous porous media. By perturbation expansions, we first derive partial differential equations governing the zeroth-order head $h^{(0)}$ and the first-order head term $h^{(1)}$, where orders are in terms of the standard deviation of the log transmissivity. We then solve $h^{(0)}$ and $h^{(1)}$ analytically, both of which are expressed as infinite series. The head perturbation $h^{(1)}$ is then used to derive expressions for autocovariance of the hydraulic head and the cross covariance between the log transmissivity and head. The expressions for the mean flux and flux covariance tensor are formulated from the head moments based on Darcy's law. Using numerical examples, we demonstrate the convergence of these solutions. We also examine the accuracy of these first-order solutions by comparing them with solutions from both Monte Carlo simulations and the numerical moment equation method.

Citation: Lu, Z., and D. Zhang (2005), Analytical solutions to statistical moments for transient flow in two-dimensional, bounded, randomly heterogeneous media, *Water Resour. Res.*, *41*, W01016, doi:10.1029/2004WR003389.

1. Introduction

[2] Geological formations are inherently heterogeneous and exhibit a high degree of variability in medium properties such as hydraulic conductivity and porosity. Medium heterogeneity has significant impacts on fluid flow and solute transport in the subsurface. Although these formations are intrinsically deterministic, we usually have incomplete knowledge on their properties. As a result, it is common to treat the medium properties as stochastic processes and solve the flow and transport problems in randomly heterogeneous media in a stochastic framework. In the last two decades, many stochastic theories have been developed to obtain the statistical moments for fluid flow and solute transport in such heterogeneous media [e.g., *Freeze*, 1975; *Smith and Freeze*, 1979; *Dagan*, 1979, 1982, 1989; *Dettinger and Wilson*, 1981; *Gutjahr and Gelhar*, 1981; *Mizell et al.*, 1982; *Gelhar and Axness*, 1983; *Rubin and Dagan*, 1989; *Neuman and Orr*, 1993; *Gelhar*, 1993; *Osnes*, 1995, 1998; *Tartakovsky and Neuman*, 1998; *Zhang*, 1999; *Guadagnini and Neuman*, 1999a, 1999b]. *Zhang* [2002] reviewed some techniques used in solving transient flow in heterogeneous porous media.

[3] Analytical solutions to the statistical moments of saturated flow are only available for some special cases such as steady state uniform mean flow in an unbounded domain [*Dagan*, 1985; *Gelhar*, 1993; *Rubin*, 1990; *Rubin and Dagan*, 1992; *Zhang and Neuman*, 1992] and steady state uniform mean flow in a rectangular domain [*Osnes*, 1995, 1998]. Under the assumption of steady state uniform mean flow in an infinite domain, *Dagan* [1985] derived an analytical solution for the head variogram with an exponential covariance function of the log hydraulic conductivity. Under similar assumptions, *Rubin and Dagan* [1992] and *Zhang and Neuman* [1992] presented solutions to velocity covariances. *Osnes* [1995, 1998] derived analytical solutions to head and velocity moments for steady state uniform mean flow in a rectangular domain with a separable exponential covariance function of the log transmissivity. Recently, *Riva et al.* [2001] and *Guadagnini et al.* [2003] derived analytical solutions for steady state radial flow in bounded heterogeneous domains. To our knowledge, analytical solutions for head and velocity moments for transient flow are not available in the literature. In this study, we present analytical solutions to head and velocity covariances for transient flow in a two-dimensional statistically homogeneous porous medium with a separable exponential covariance function of the log transmissivity. We assume that the boundary conditions are deterministic and the only source of uncertainty is the variability of transmissivity. It is also assumed that the flow is initially under steady state and the initial head uncertainty is unknown (to be determined later) rather than specified in advance.

2. Mathematical Derivation

2.1. Statement of the Problem

[4] We consider transient flow in saturated two-dimensional bounded randomly heterogeneous porous media governed by the following continuity equation and Darcy's law

0043-1397/05/2004WR003389$09.00

$$\nabla \cdot \mathbf{q}(\mathbf{x},t) = S\frac{\partial h(\mathbf{x},t)}{\partial t}, \qquad \mathbf{x}\in\Omega,\ t>0 \tag{1}$$

$$\mathbf{q}(\mathbf{x},t) = -T(\mathbf{x})\nabla h(\mathbf{x},t), \tag{2}$$

with boundary and initial conditions

$$h(\mathbf{x},t) = H_1, \qquad x_1 = 0, \quad t>0, \tag{3a}$$

$$h(\mathbf{x},t) = H_2, \qquad x_1 = L_1, \quad t>0, \tag{3b}$$

$$\partial h(\mathbf{x},t)/\partial x_2 = 0, \qquad x_2 = 0, \quad t>0, \tag{3c}$$

$$\partial h(\mathbf{x},t)/\partial x_2 = 0, \qquad x_2 = L_2, \quad t>0, \tag{3d}$$

$$h(\mathbf{x},t) = H_0(\mathbf{x}), \quad \mathbf{x}\in\Omega, \quad t=0, \tag{3e}$$

where $h(\mathbf{x}, t)$ is the hydraulic head, $q(\mathbf{x}, t)$ is the specific discharge, H_1 and H_2 are prescribed constant heads, $H_0(\mathbf{x})$ is the initial head in the domain Ω, T is the transmissivity, S is storativity, $\mathbf{x} = (x_1, x_2)$ is the vector of Cartesian coordinates, L_1 and L_2 are the lengths of the flow domain in x_1 and x_2 directions, and t is time. Here we assume that H_1 and H_2 are deterministic constants while $H_0(\mathbf{x})$ is specified with uncertainty: $H_0(\mathbf{x}) = \langle H_0(\mathbf{x})\rangle + H_0'(\mathbf{x})$ where $\langle H_0\rangle$ and $H_0'(\mathbf{x})$ are respectively the mean and perturbation. It is also assumed that S is a deterministic constant whereas T is a spatially correlated stationary random function following a lognormal distribution, and we work with the log-transformed variable $Y(\mathbf{x}) = \ln[T(\mathbf{x})] = \langle Y\rangle + Y'(\mathbf{x})$, where $\langle Y\rangle$ and $Y'(\mathbf{x})$ are the mean and the perturbation of the log transmissivity, respectively. Accordingly, the hydraulic head and flux are also random functions and can be decomposed as $h(\mathbf{x}, t) = h^{(0)}(\mathbf{x}, t) + h^{(1)}(\mathbf{x}, t) + \cdots$, $\mathbf{q}(\mathbf{x}, t) = \mathbf{q}^{(0)}(\mathbf{x}, t) + \mathbf{q}^{(1)}(\mathbf{x}, t) + \cdots$, where the order of each term in this series is in terms of σ_Y, the standard deviation of the log transmissivity. Our aim is to solve for the statistics (mean and covariance) of head and flux.

2.2. First-Order Mean Head and Mean Flux

[5] Upon combining (1) and (2), substituting decompositions of $h(\mathbf{x}, t)$, $H_0(\mathbf{x})$, and $T(\mathbf{x}) = \exp(Y(\mathbf{x})) \approx T_G[1 + Y'(\mathbf{x})]$, where T_G is the geometric mean of transmissivity, into the derived equation with boundary and initial conditions (3), and collecting terms at zeroth order, one obtains the following equation:

$$\frac{\partial^2 h^{(0)}(\mathbf{x},t)}{\partial x_1^2} + \frac{\partial^2 h^{(0)}(\mathbf{x},t)}{\partial x_2^2} = \frac{S}{T_G}\frac{\partial h^{(0)}(\mathbf{x},t)}{\partial t}, \ \mathbf{x}\in\Omega, \quad t>0, \tag{4}$$

with boundary and initial conditions

$$h^{(0)}(\mathbf{x},t) = H_1, \qquad x_1 = 0, \quad t>0, \tag{5a}$$

$$h^{(0)}(\mathbf{x},t) = H_2, \qquad x_1 = L_1, \quad t>0, \tag{5b}$$

$$\partial h^{(0)}(\mathbf{x},t)/\partial x_2 = 0, \qquad x_2 = 0, \quad t>0, \tag{5c}$$

$$\partial h^{(0)}(\mathbf{x},t)/\partial x_2 = 0, \qquad x_2 = L_2, \quad t>0, \tag{5d}$$

$$h^{(0)}(\mathbf{x},0) = \langle H_0(\mathbf{x})\rangle, \qquad \mathbf{x}\in\Omega. \tag{5e}$$

Certainly, the first-order transient mean head depends on the initial mean head. Here we choose a special case: $\langle H_0(\mathbf{x})\rangle = H_{10} + (H_{20} - H_{10})x_1/L_1$, i.e., assuming a steady state initial condition with initial gradient of $J_0 = (H_{10} - H_{20})/L_1$. At time $t = 0$, the head values at two constant head boundaries are changed to H_1 and H_2, respectively. The solution to (4)–(5) for such a scenario can be expressed as an infinite series (Appendix A):

$$h^{(0)}(\mathbf{x},t) = \frac{2}{L_1}\sum_{m=1}^{\infty}\frac{\sin(\alpha_m x_1)}{\alpha_m}\Big[\Big(H_{10} - (-1)^m H_{20}\Big)\, e^{-\frac{T_G}{S}\alpha_m^2 t} + (H_1 - (-1)^m H_2)\Big(1 - e^{-\frac{T_G}{S}\alpha_m^2 t}\Big)\Big], \tag{6}$$

where $\alpha_m = m\pi/L_1$, $m = 1, 2, \cdots$. Each term in this series is a weighted average of the effect of the constant head boundaries at time $t = 0$ and $t > 0$. Utilizing the identities $\sum_{k=1}^{\infty}\sin(kz)/k = (\pi - z)/2$ for $0 < z < 2\pi$ and $\sum_{k=1}^{\infty}(-1)^{k-1}\sin(kz)/k = z/2$ for $-\pi < z < \pi$, it can be verified that for $t = 0$ and $t = \infty$, (6) reduces to $h^{(0)}(\mathbf{x}, 0) = H_{10} + (H_{20} - H_{10})x_1/L_1$ and $h^{(0)}(\mathbf{x}, \infty) = H_1 + (H_2 - H_1)x_1/L_1$. For any time $0 < t < \infty$, $h^{(0)}(\mathbf{x}, t)$ has to be evaluated numerically. Since $\sin(\alpha_m x_1) = 0$ at two constant head boundaries $x_1 = 0$ and $x_1 = L_1$, the value of any truncated finite summation of (6) at these two constant head boundaries will be zero. To avoid this, we may rewrite (6) in an alternative form:

$$h^{(0)}(\mathbf{x},t) = H_1 + \frac{H_2 - H_1}{L_1}x_1 + \frac{2}{L_1}\sum_{m=1}^{\infty}\frac{b_m\sin(\alpha_m x_1)}{\alpha_m}e^{-\frac{T_G}{S}\alpha_m^2 t}, \tag{7}$$

where $b_m = (H_{10} - H_1) - (-1)^m(H_{20} - H_2)$. Note that the terms in the series of (7) are dampened exponentially with a rate coefficient of $T_G\alpha_m^2/S$ and thus the solution can be approximated by keeping only those terms with a high spectral density. For a large time t, only a few leading terms are required to approximate the solution because these leading terms account for most of the spectral density. On the other hand, for time $t \to 0$, a large number of terms are needed to accurately approximate the solution.

[6] Similarly, after substituting decompositions of $\mathbf{q}(\mathbf{x}, t)$, $h(\mathbf{x}, t)$, and $Y(\mathbf{x})$ into (2) and collecting terms at the zeroth order, one has

$$\mathbf{q}^{(0)}(\mathbf{x},t) = -T_G\nabla h^{(0)}(\mathbf{x},t), \tag{8}$$

or, by utilizing (7), one has the following expressions for the flux components:

$$q_1^{(0)}(\mathbf{x},t) = T_G\left[J_1 - \frac{2}{L_1}\sum_{m=1}^{\infty}b_m\cos(\alpha_m x_1)e^{-\frac{T_G}{S}\alpha_m^2 t}\right]$$
$$q_2^{(0)}(\mathbf{x},t) = 0, \tag{9}$$

where $J_1 = (H_1 - H_2)/L_1$ is the final steady state mean hydraulic gradient.

2.3. First-Order Head Perturbations

[7] The equation for the first-order term $h^{(1)}$ reads

$$\frac{\partial^2 h^{(1)}(\mathbf{x},t)}{\partial x_i^2} + \frac{\partial}{\partial x_i}\left(Y'(\mathbf{x})\frac{\partial h^{(0)}(\mathbf{x})}{\partial x_i}\right) = \frac{S}{T_G}\frac{\partial h^{(1)}(\mathbf{x},t)}{\partial t}, \qquad \mathbf{x}\in\Omega, \quad t>0, \tag{10}$$

where summation over repeated index is implied. Boundary and initial conditions corresponding to (10) are

$$h^{(1)}(\mathbf{x},t)=0, \qquad x_1=0 \quad \text{or} \quad x_1=L_1, \quad t>0, \tag{11a}$$

$$\partial h^{(1)}(\mathbf{x},t)/\partial x_2=0, \quad x_2=0 \quad \text{or} \quad x_2=L_2, \quad t>0, \tag{11b}$$

$$h^{(1)}(\mathbf{x},0)=H_0'(\mathbf{x}) \qquad \mathbf{x}\in\Omega. \tag{11c}$$

[8] We have to emphasize that the perturbation of the initial head $H_0'(\mathbf{x})$ depends on the variability of $Y(\mathbf{x})$ and therefore cannot be arbitrarily assigned. By assuming that the flow system is initially in steady state, the functional form of the unknown initial perturbation can be determined later. Equations (10)–(11) can be solved analytically (Appendix B) and the solution is

$$\begin{aligned} h^{(1)}(\mathbf{x},t) = {} & \frac{4}{D}\sum_{\substack{m=1\\n=0}}^{\infty} a_n \sin(\alpha_m x_1)\cos(\beta_n x_2) e^{-\frac{T_G}{S}\left(\alpha_m^2+\beta_n^2\right)t} \\ & \cdot \int_\Omega H_0'(\mathbf{x}')\sin\left(\alpha_m x_1'\right)\cos\left(\beta_n x_2'\right)d\mathbf{x}' \\ & + \frac{4J_1}{D}\sum_{\substack{m=1\\n=0}}^{\infty} \frac{a_n\alpha_m \sin(\alpha_m x_1)\cos(\beta_n x_2)}{\alpha_m^2+\beta_n^2} \\ & \cdot \left[1-e^{-\frac{T_G}{S}\left(\alpha_m^2+\beta_n^2\right)t}\right]\int_\Omega Y'(\mathbf{x}')\cos\left(\alpha_m x_1'\right) \\ & \cdot \cos\left(\beta_n x_2'\right)d\mathbf{x}' - \frac{8T_G}{DL_1S}\sum_{\substack{m,k=1\\n=0}}^{\infty} a_n b_k P_{kmn}(t)\alpha_m \\ & \cdot \sin(\alpha_m x_1)\cos(\beta_n x_2)\int_\Omega Y'(\mathbf{x}')\cos\left(\alpha_m x_1'\right)\cos\left(\alpha_k x_1'\right) \\ & \cdot \cos\left(\beta_n x_2'\right)d\mathbf{x}', \end{aligned} \tag{12}$$

where $\beta_n = n\pi/L_2$, $n = 0, 1, 2, \ldots$, $a_n = 1$ for $n > 0$ and $a_n = 1/2$ for $n = 0$, terms b_k and $P_{kmn}(t)$ are defined in Appendix B. Since $P_{kmn}(0) = 0$, it can be verified that $h^{(1)}(\mathbf{x}, 0) = H'(\mathbf{x})$. By taking the limit of (12) as $t \to \infty$, one obtains the steady state solution of the head perturbation:

$$\begin{aligned} h^{(1)}(\mathbf{x},\infty) = {} & \frac{4J_1}{D}\sum_{\substack{m=1\\n=0}}^{\infty} \frac{a_n\alpha_m \sin(\alpha_m x_1)\cos(\beta_n x_2)}{\alpha_m^2+\beta_n^2}\int_\Omega Y'(\mathbf{x}') \\ & \cdot \cos\left(\alpha_m x_1'\right)\cos\left(\beta_n x_2'\right)d\mathbf{x}'. \end{aligned} \tag{13}$$

In particular, the initial head perturbation $H_0'(\mathbf{x})$ can be written as

$$\begin{aligned} H_0'(\mathbf{x}) = {} & \frac{4J_0}{D}\sum_{\substack{m=1\\n=0}}^{\infty} \frac{a_n\alpha_m \sin(\alpha_m x_1)\cos(\beta_n x_2)}{\alpha_m^2+\beta_n^2}\int_\Omega Y'(\mathbf{x}') \\ & \cdot \cos\left(\alpha_m x_1'\right)\cos\left(\beta_n x_2'\right)d\mathbf{x}', \end{aligned} \tag{14}$$

which will be used to formulate the (cross) covariance C_{YH_0} and C_{H_0} that are required in solving for transient head covariances.

2.4. Steady State Second Moments of Head

[9] The cross covariance between the log transmissivity and the steady state hydraulic head can be obtained by writing (13) in terms of a reference point $\mathbf{y}$, multiplying $Y'(\mathbf{x})$ to the resulting equation, and taking the mean,

$$\begin{aligned} C_{Yh}(\mathbf{x},\mathbf{y}) &= \left\langle Y'(\mathbf{x})\, h^{(1)}(\mathbf{y},\infty)\right\rangle \\ &= \frac{4J_1}{D}\sum_{\substack{m=1\\n=0}}^{\infty} \frac{a_n\alpha_m \sin(\alpha_m y_1)\cos(\beta_n y_2)}{\alpha_m^2+\beta_n^2} R_{mn}(\mathbf{x}), \end{aligned} \tag{15}$$

where $R_{mn}(\mathbf{x}) = \int_\Omega C_Y(\mathbf{x}, \mathbf{x}')\cos(\alpha_m x_1')\cos(\beta_n x_2')d\mathbf{x}'$, and $C_Y(\mathbf{x}, \mathbf{x}') = \langle Y'(\mathbf{x})Y'(\mathbf{x}')\rangle$ is the covariance of the log transmissivity Y. As done by *Osnes* [1995] and *Rubin and Dagan* [1988], we choose C_Y as a separable exponential function:

$$C_Y(\mathbf{x},\mathbf{x}') = \sigma_Y^2 \exp\left(-\frac{\left|x_1-x_1'\right|}{\lambda_1}-\frac{\left|x_2-x_2'\right|}{\lambda_2}\right), \tag{16}$$

where σ_Y^2 is the variance of Y, and λ_1 and λ_2 are the correlation lengths of Y in x_1 and x_2 directions, respectively. For this particular covariance function, $R_{mn}(\mathbf{x})$ can be found analytically:

$$\begin{aligned} R_{mn}(\mathbf{x}) = {} & \frac{\lambda_1\lambda_2\sigma_Y^2}{\left(\alpha_m^2\lambda_1^2+1\right)\left(\beta_n^2\lambda_2^2+1\right)} \\ & \cdot \left[2\cos(\alpha_m x_1) - e^{-x_1/\lambda_1} - (-1)^m e^{(x_1-L_1)/\lambda_1}\right] \\ & \times \left[2\cos(\beta_n x_2) - e^{-x_2/\lambda_2} - (-1)^n e^{(x_2-L_2)/\lambda_2}\right]. \end{aligned} \tag{17}$$

The steady state head covariance can be derived by multiplying $h^{(1)}(\mathbf{y}, \infty)$ to (13), taking the mean, and substituting (15) into the derived equation

$$\begin{aligned} C_h(\mathbf{x},\mathbf{y}) = {} & \frac{16J_1^2}{D^2}\sum_{\substack{m,m_1=1\\n,n_1=0}}^{\infty} \\ & \cdot \frac{a_n a_{n_1}\alpha_m\alpha_{m_1}\sin(\alpha_m x_1)\cos(\beta_n x_2)\sin(\alpha_{m_1} y_1)\cos\left(\beta_{n_1} y_2\right)}{\left(\alpha_m^2+\beta_n^2\right)\left(\alpha_{m_1}^2+\beta_{n_1}^2\right)} \\ & \cdot Q_{m_1 n_1}^{mn}, \end{aligned} \tag{18}$$

where

$$\begin{aligned} Q_{m_1 n_1}^{mn} = {} & \int_\Omega R_{m_1 n_1}(\mathbf{x}')\cos\left(\alpha_m x_1'\right)\cos\left(\beta_n x_2'\right)d\mathbf{x}' \\ = {} & \frac{\lambda_1\lambda_2\sigma_Y^2}{\left(\alpha_{m_1}^2\lambda_1^2+1\right)\left(\beta_{n_1}^2\lambda_2^2+1\right)} \\ & \cdot \left[L_1\delta_{mm_1} + \frac{\lambda_1}{\alpha_m^2\lambda_1^2+1}\left[1+(-1)^{m+m_1}\right]\left[(-1)^m e^{-L_1/\lambda_1}-1\right]\right] \\ & \cdot \left[\left(\delta_{nn_1}+\delta_{n0}\delta_{n_1 0}\right)L_2 + \frac{\lambda_2}{\beta_n^2\lambda_2^2+1}\left[1+(-1)^{n+n_1}\right]\left[(-1)^n e^{-L_2/\lambda_2}-1\right]\right] \end{aligned} \tag{19}$$

and δ_{ij} is the Kronecker delta function.

[10] Equation (18) leads to the steady state head variance

$$\begin{aligned} \sigma_h^2(\mathbf{x}) = {} & \frac{16J_1^2}{D^2}\sum_{\substack{m,m_1=1\\n,n_1=0}}^{\infty} \\ & \cdot \frac{a_n a_{n_1}\alpha_m\alpha_{m_1}\sin(\alpha_m x_1)\cos(\beta_n x_2)\sin(\alpha_{m_1} x_1)\cos\left(\beta_{n_1} x_2\right)}{\left(\alpha_m^2+\beta_n^2\right)\left(\alpha_{m_1}^2+\beta_{n_1}^2\right)} \\ & \cdot Q_{m_1 n_1}^{mn}. \end{aligned} \tag{20}$$

Certainly, the expressions for the head covariance and head variance, i.e., (18) and (20), are much simpler than those of

Osnes [1995, equations (14)–(15)]. Note that the expressions for the cross covariance $\langle Y'(\mathbf{x})H_0'(\mathbf{y})\rangle$ and autocovariance $C_{H_0}(\mathbf{x}, \mathbf{y})$ can be written similarly as (15) and (18), simply replacing J_1 in these equations by the initial hydraulic gradient J_0.

[11] From (19) and (20), it is seen that the steady state head variance is proportional to σ_Y^2, as expected. However, the dependence of the head variance on the correlation lengths is not obvious. For the case of $\lambda_1 \to 0$ and $\lambda_2 \to 0$, which corresponds to the case with a white noise covariance function, it is easy to find from (C7) that $Q_{m1n1}^{mn} \to 0$ and thus the head variance is zero. This is consistent with the results of *Dagan* [1985] for an exponential covariance function in an unbounded domain. For the case with large correlation lengths, if the field is isotropic, one finds from (19) that $\lim_{\lambda_1=\lambda_2\to 0} Q_{m1n1}^{mn} = 0$ and the head variance is zero. As a matter of the fact, the transmissivity field in this case becomes a random constant, which results in a zero head variance everywhere in the domain. Unlike the case of an isotropic covariance function in an unbounded domain, in which the head variance increases from zero to infinity as the correlation length increases from zero to infinity, for a bounded isotropic domain the head variance increases from zero to a certain value as the correlation length increases and then decreases to zero again as the correlation length approaches infinity. This phenomenon has been observed in the previous study [*Zhang and Lu*, 2004, Figure 3].

[12] Equations (19) and (20) can also be used to analyze the behaviors of the head variance for the anisotropic field. For the case with a fixed λ_2 and for $\lambda_1 \to \infty$, which is the case of bedding parallel to the mean flow direction, it can be shown that $Q_{m1n1}^{mn} \to 0$ and the head variance is zero. However, for a fixed λ_1 and $\lambda_2 \to \infty$ (bedding perpendicular to the mean flow, the head variance computed from (20) is infinity.

2.5. Transient Second Moments of Head

[13] The transient cross covariance $C_{Yh}(\mathbf{x}; \mathbf{y}, \tau)$ and $C_h(\mathbf{x}, t; \mathbf{y}, \tau)$ can be derived from (12) as (see Appendix C)

$$C_{Yh}(\mathbf{x};\mathbf{y},\tau) = \frac{4}{D}\sum_{\substack{m=1\\n=0}}^{\infty}\frac{a_n\alpha_m\sin(\alpha_m y_1)\cos(\beta_n y_2)}{\alpha_m^2+\beta_n^2}R_{mn}(\mathbf{x})J_{mn}(\tau) - \frac{8T_G}{DL_1S}\sum_{\substack{m,k=1\\n=0}}^{\infty}a_n b_k P_{kmn}(\tau)\alpha_m\sin(\alpha_m y_1)\cos(\beta_n y_2)\cdot R_{kmn}(\mathbf{x}), \quad (21)$$

$$C_h(\mathbf{x},t;\mathbf{y},\tau) = \frac{16}{D^2}\sum_{\substack{m,m_1=1\\n,n_1=0}}^{\infty}\frac{a_n a_{n_1}\alpha_m\alpha_{m_1}Q_{mn}^{m_1n_1}SC}{\left(\alpha_m^2+\beta_n^2\right)\left(\alpha_{m_1}^2+\beta_{n_1}^2\right)}J_{mn}(t)J_{m_1n_1}(\tau) - \frac{32T_G}{D^2L_1S}\sum_{\substack{m,m_1,k_1=1\\n,n_1=0}}^{\infty}\frac{a_n a_{n_1}\alpha_m\alpha_{m_1}b_{k_1}P_{k_1m_1n_1}(\tau)\,SC}{\alpha_m^2+\beta_n^2}\cdot Q_{mn}^{k_1m_1n_1}J_{mn}(t) - \frac{32T_G}{D^2L_1S}\sum_{\substack{m,m_1,k=1\\n,n_1=0}}^{\infty}\cdot\frac{a_n a_{n_1}\alpha_m\alpha_{m_1}b_k P_{kmn}(t)SC}{\alpha_{m_1}^2+\beta_{n_1}^2}Q_{m_1n_1}^{kmn}J_{m_1n_1}(\tau) + \frac{64T_G^2}{D^2L_1^2S^2}\cdot\sum_{\substack{m,m_1,k,k_1=1\\n,n_1=0}}^{\infty}a_n a_{n_1}\alpha_m\alpha_{m_1}b_k b_{k_1}P_{kmn}(t)P_{k_1m_1n_1}(\tau)\cdot SC\,Q_{kmn}^{k_1m_1n_1}, \quad (22)$$

where

$$SC = \sin(\alpha_m y_1)\cos(\beta_n y_2)\sin(\alpha_{m_1}x_1)\cos\left(\beta_{n_1}x_2\right), \quad (23)$$

$$J_{mn}(t) = \left[J_1 + (J_0 - J_1)e^{-\frac{T_G}{S}\left(\alpha_m^2+\beta_n^2\right)t}\right], \quad (24)$$

and all other terms are given in Appendix C. By taking the limit as $t \to \infty$, (21) and (22) reduce to (15) and (18).

2.6. Second Moments of Flux

[14] The first-order flux can be written as

$$\mathbf{q}^{(1)}(\mathbf{x},t) = -T_G\nabla h^{(1)}(\mathbf{x},t) + Y'(\mathbf{x})\mathbf{q}^{(0)}(\mathbf{x},t) \quad (25)$$

or in the component form

$$q_i^{(1)}(\mathbf{x},t) = -T_G\frac{\partial h^{(1)}(\mathbf{x},t)}{\partial x_i} + Y'(\mathbf{x})q_i^{(0)}(\mathbf{x},t), \quad i = 1,2. \quad (26)$$

Multiplying $Y'(\mathbf{y})$ on (26) and taking the mean yields

$$C_{Yq_i}(\mathbf{y};\mathbf{x},t) = \langle Y'(\mathbf{y})q_i^{(1)}(\mathbf{x},t)\rangle = -T_G\frac{\partial C_{Yh}(\mathbf{y};\mathbf{x},t)}{\partial x_i} + q_i^{(0)}(\mathbf{x},t)C_Y(\mathbf{x},\mathbf{y}). \quad (27)$$

More specifically, (27) can be expanded as

$$C_{Yq_1}(\mathbf{y};\mathbf{x},t) = q_1^{(0)}(\mathbf{x},t)C_Y(\mathbf{x},\mathbf{y}) - \frac{4T_G}{D}\sum_{\substack{m=1\\n=0}}^{\infty}\cdot\frac{a_n\alpha_m^2\cos(\alpha_m x_1)\cos(\beta_n x_2)}{\alpha_m^2+\beta_n^2}R_{mn}(\mathbf{y})J_{mn}(t) + \frac{8T_G^2}{DL_1S}\sum_{\substack{m,k=1\\n=0}}^{\infty}a_n b_k\alpha_m^2P_{kmn}(t)\cos(\alpha_m x_1)\cos(\beta_n x_2)\cdot R_{kmn}(\mathbf{y}) \quad (28)$$

and

$$C_{Yq_2}(\mathbf{y};\mathbf{x},t) = \frac{4T_G}{D}\sum_{\substack{m=1\\n=0}}^{\infty}\frac{a_n\alpha_m\beta_n\sin(\alpha_m x_1)\sin(\beta_n x_2)}{\alpha_m^2+\beta_n^2}\cdot R_{mn}(\mathbf{y})J_{mn}(t) - \frac{8T_G^2}{DL_1S}\sum_{\substack{m,k=1\\n=0}}^{\infty}a_n b_k\alpha_m\beta_n P_{kmn}(t)\cdot\sin(\alpha_m x_1)\sin(\beta_n x_2)R_{kmn}(\mathbf{y}). \quad (29)$$

The flux covariance $q_{ij}(\mathbf{x}, t; \mathbf{y}, \tau) = \langle q_i^{(1)}(\mathbf{x}, t)q_j^{(1)}(\mathbf{y}, \tau)\rangle$ can be derived from (26):

$$q_{ij}(\mathbf{x},t;\mathbf{y},\tau) = T_G^2\frac{\partial^2 C_h(\mathbf{x},t;\mathbf{y},\tau)}{\partial x_i\partial y_j} - T_G\,q_j^{(0)}(\mathbf{y},\tau)\frac{\partial C_{Yh}(\mathbf{y};\mathbf{x},t)}{\partial x_i} - T_G\,q_i^{(0)}(\mathbf{x},t)\frac{\partial C_{Yh}(\mathbf{x};\mathbf{y},\tau)}{\partial y_j} + q_i^{(0)}(\mathbf{x},t)\,q_j^{(0)}(\mathbf{y},\tau)\cdot C_Y(\mathbf{x},\mathbf{y}), i,j = 1,2, \quad (30)$$

which can be elaborated as

$$
\begin{aligned}
q_{11}(\mathbf{x},t;\mathbf{y},\tau) = {} & \frac{16T_G^2}{D^2}\sum_{\substack{m,m_1=1\\ n,n_1=0}}^{\infty}\frac{a_n a_{n_1}\alpha_m^2\alpha_{m_1}^2 Q_{mn}^{m_1n_1} CC}{\left(\alpha_m^2+\beta_n^2\right)\left(\alpha_{m_1}^2+\beta_{n_1}^2\right)}J_{mn}(t)J_{m_1n_1}(\tau)\\
& -\frac{32T_G^3}{D^2L_1S}\sum_{\substack{m,m_1,k_1=1\\ n,n_1=0}}^{\infty}\frac{a_n a_{n_1}\alpha_m^2\alpha_{m_1}^2 b_{k_1}P_{k_1m_1n_1}(\tau)\,CC}{\alpha_m^2+\beta_n^2}\\
& \cdot Q_{mn}^{k_1m_1n_1}J_{mn}(t) - \frac{32T_G^3}{D^2L_1S}\sum_{\substack{m,m_1,k=1\\ n,n_1=0}}^{\infty}\\
& \cdot\frac{a_n a_{n_1}\alpha_m^2\alpha_{m_1}^2 b_k P_{kmn}(t)CC}{\alpha_{m_1}^2+\beta_{n_1}^2}Q_{m_1n_1}^{kmn}J_{m_1n_1}(\tau)\\
& +\frac{64T_G^4}{D^2L_1^2S^2}\sum_{\substack{m,m_1,k,k_1=1\\ n,n_1=0}}^{\infty}a_n a_{n_1}\alpha_m^2\alpha_{m_1}^2 b_k b_{k_1}P_{kmn}(t)\\
& \cdot P_{k_1m_1n_1}(\tau)CC\,Q_{kmn}^{k_1m_1n_1} - \frac{4T_G\,q_1^{(0)}(\mathbf{y},\tau)}{D}\sum_{\substack{m=1\\ n=0}}^{\infty}\\
& \cdot\frac{a_n\alpha_m^2\cos(\alpha_m x_1)\cos(\beta_n x_2)}{\alpha_m^2+\beta_n^2}R_{mn}(\mathbf{y})J_{mn}(t)\\
& +\frac{8T_G^2\,q_1^{(0)}(\mathbf{y},\tau)}{DL_1S}\sum_{\substack{m,k=1\\ n=0}}^{\infty}a_n b_k P_{kmn}(t)\alpha_m^2\cos(\alpha_m x_1)\\
& \cdot\cos(\beta_n x_2)R_{kmn}(\mathbf{y}) - \frac{4T_G\,q_1^{(0)}(\mathbf{x},t)}{D}\sum_{\substack{m=1\\ n=0}}^{\infty}\\
& \cdot\frac{a_n\alpha_m^2\cos(\alpha_m y_1)\cos(\beta_n y_2)}{\alpha_m^2+\beta_n^2}R_{mn}(\mathbf{x})J_{mn}(\tau)\\
& +\frac{8T_G^2\,q_1^{(0)}(\mathbf{x},t)}{DL_1S}\sum_{\substack{m,k=1\\ n=0}}^{\infty}a_n b_k P_{kmn}(\tau)\alpha_m^2\cos(\alpha_m y_1)\\
& \cdot\cos(\beta_n y_2)R_{kmn}(\mathbf{x}) + q_1^{(0)}(\mathbf{x},t)\,q_1^{(0)}(\mathbf{y},\tau)\\
& \cdot C_Y(\mathbf{x},\mathbf{y}),
\end{aligned}
\tag{31}
$$

$$
\begin{aligned}
q_{12}(\mathbf{x},t;\mathbf{y},\tau) = {} & -\frac{16T_G^2}{D^2}\sum_{\substack{m,m_1=1\\ n,n_1=0}}^{\infty}\frac{a_n a_{n_1}\alpha_m\alpha_{m_1}^2\beta_n Q_{mn}^{m_1n_1} SC}{\left(\alpha_m^2+\beta_n^2\right)\left(\alpha_{m_1}^2+\beta_{n_1}^2\right)}J_{mn}(t)\\
& \cdot J_{m_1n_1}(\tau) + \frac{32T_G^3}{D^2L_1S}\sum_{\substack{m,m_1,k_1=1\\ n,n_1=0}}^{\infty}\\
& \cdot\frac{a_n a_{n_1}\alpha_m\beta_n\alpha_{m_1}^2 b_{k_1}P_{k_1m_1n_1}(\tau)\,SC}{\alpha_m^2+\beta_n^2}Q_{mn}^{k_1m_1n_1}J_{mn}(t)\\
& +\frac{32T_G^3}{D^2L_1S}\sum_{\substack{m,m_1,k=1\\ n,n_1=0}}^{\infty}\frac{a_n a_{n_1}\alpha_m\alpha_{m_1}^2\beta_n b_k P_{kmn}(t)SC}{\alpha_{m_1}^2+\beta_{n_1}^2}\\
& \cdot Q_{m_1n_1}^{kmn}J_{m_1n_1}(\tau) - \frac{64T_G^4}{D^2L_1^2S^2}\sum_{\substack{m,m_1,k,k_1=1\\ n,n_1=0}}^{\infty}\\
& \cdot a_n a_{n_1}\alpha_m\alpha_{m_1}^2\beta_n b_k b_{k_1}P_{kmn}(t)P_{k_1m_1n_1}(\tau)SC\,Q_{kmn}^{k_1m_1n_1}\\
& +\frac{4T_G\,q_1^{(0)}(\mathbf{x},t)}{D}\sum_{\substack{m=1\\ n=0}}^{\infty}\frac{a_n\alpha_m\beta_n\sin(\alpha_m y_1)\sin(\beta_n y_2)}{\alpha_m^2+\beta_n^2}\\
& \cdot R_{mn}(\mathbf{x})J_{mn}(\tau) - \frac{8T_G^2\,q_1^{(0)}(\mathbf{x},t)}{DL_1S}\sum_{\substack{m,k=1\\ n=0}}^{\infty}a_n b_k P_{kmn}(\tau)\\
& \cdot\alpha_m\beta_n\sin(\alpha_m y_1)\sin(\beta_n y_2)R_{kmn}(\mathbf{x}),
\end{aligned}
\tag{32}
$$

and

$$
\begin{aligned}
q_{22}(\mathbf{x},t;\mathbf{y},\tau) = {} & \frac{16T_G^2}{D^2}\sum_{\substack{m,m_1=1\\ n,n_1=0}}^{\infty}\frac{a_n a_{n_1}\alpha_m\alpha_{m_1}\beta_n\beta_{n_1}Q_{mn}^{m_1n_1}SS}{\left(\alpha_m^2+\beta_n^2\right)\left(\alpha_{m_1}^2+\beta_{n_1}^2\right)}J_{mn}(t)\\
& \cdot J_{m_1n_1}(\tau) - \frac{32T_G^3}{D^2L_1S}\sum_{\substack{m,m_1,k_1=1\\ n,n_1=0}}^{\infty}\\
& \cdot\frac{a_n a_{n_1}\alpha_m\alpha_{m_1}\beta_n\beta_{n_1}b_{k_1}P_{k_1m_1n_1}(\tau)SS}{\alpha_m^2+\beta_n^2}Q_{mn}^{k_1m_1n_1}J_{mn}(t)\\
& -\frac{32T_G^3}{D^2L_1S}\sum_{\substack{m,m_1,k=1\\ n,n_1=0}}^{\infty}\frac{a_n a_{n_1}\alpha_m\alpha_{m_1}\beta_n\beta_{n_1}b_k P_{kmn}(t)SS}{\alpha_{m_1}^2+\beta_{n_1}^2}\\
& \cdot Q_{m_1n_1}^{kmn}J_{m_1n_1}(\tau) + \frac{64T_G^4}{D^2L_1^2S^2}\sum_{\substack{m,m_1,k,k_1=1\\ n,n_1=0}}^{\infty}\\
& \cdot a_n a_{n_1}\alpha_m\alpha_{m_1}\beta_n\beta_{n_1}b_k b_{k_1}P_{kmn}(t)P_{k_1m_1n_1}(\tau)\\
& \cdot SSQ_{kmn}^{k_1m_1n_1},
\end{aligned}
\tag{33}
$$

where

$$
\begin{aligned}
SC &= \sin(\alpha_m y_1)\sin(\beta_n y_2)\cos(\alpha_{m_1}x_1)\cos\left(\beta_{n_1}x_2\right),\\
CC &= \cos(\alpha_m y_1)\cos(\beta_n y_2)\cos(\alpha_{m_1}x_1)\cos\left(\beta_{n_1}x_2\right),\\
SS &= \sin(\alpha_m y_1)\sin(\beta_n y_2)\sin(\alpha_{m_1}x_1)\sin\left(\beta_{n_1}x_2\right).
\end{aligned}
\tag{34}
$$

The expression for q_{21} has been omitted, because of the fact $q_{21}(\mathbf{x}, t; \mathbf{y}, \tau) \equiv q_{12}(\mathbf{y}, \tau; \mathbf{x}, t)$. Since $q_1(\mathbf{x}, \infty) = T_G J_1$ and $J_{mn}(\infty) = J_1$, the steady state flux covariance can be written from (31) to (33) as

$$
\begin{aligned}
q_{11}(\mathbf{x};\mathbf{y}) = {} & \frac{16T_G^2J_1^2}{D^2}\sum_{\substack{m,m_1=1\\ n,n_1=0}}^{\infty}\frac{a_n a_{n_1}\alpha_m^2\alpha_{m_1}^2 Q_{mn}^{m_1n_1}}{\left(\alpha_m^2+\beta_n^2\right)\left(\alpha_{m_1}^2+\beta_{n_1}^2\right)}\cos(\alpha_m y_1)\\
& \cdot\cos(\beta_n y_2)\cos(\alpha_{m_1}x_1)\cos\left(\beta_{n_1}x_2\right) - \frac{4T_G^2J_1^2}{D}\sum_{\substack{m=1\\ n=0}}^{\infty}\\
& \cdot\frac{a_n\alpha_m^2}{\alpha_m^2+\beta_n^2}\left[R_{mn}(\mathbf{x})\cos(\alpha_m y_1)\cos(\beta_n y_2)\right.\\
& \left.+\,R_{mn}(\mathbf{y})\cos(\alpha_m x_1)\cos(\beta_n x_2)\right] + T_G^2J_1^2\,C_Y(\mathbf{x},\mathbf{y}),
\end{aligned}
\tag{35}
$$

$$
\begin{aligned}
q_{12}(\mathbf{x};\mathbf{y}) = {} & -\frac{16T_G^2J_1^2}{D^2}\sum_{\substack{m,m_1=1\\ n,n_1=0}}^{\infty}\frac{a_n a_{n_1}\alpha_m\alpha_{m_1}^2\beta_n Q_{mn}^{m_1n_1}}{\left(\alpha_m^2+\beta_n^2\right)\left(\alpha_{m_1}^2+\beta_{n_1}^2\right)}\sin(\alpha_m y_1)\\
& \cdot\sin(\beta_n y_2)\cos(\alpha_{m_1}x_1)\cos\left(\beta_{n_1}x_2\right) + \frac{4T_G^2J_1^2}{D}\sum_{\substack{m=1\\ n=0}}^{\infty}\\
& \cdot\frac{a_n\alpha_m\beta_n\sin(\alpha_m y_1)\sin(\beta_n y_2)}{\alpha_m^2+\beta_n^2}R_{mn}(\mathbf{x}),
\end{aligned}
\tag{36}
$$

and

$$
\begin{aligned}
q_{22}(\mathbf{x};\mathbf{y}) = {} & \frac{16T_G^2J_1^2}{D^2}\sum_{\substack{m,m_1=1\\ n,n_1=0}}^{\infty}\frac{a_n a_{n_1}\alpha_m\alpha_{m_1}\beta_n\beta_{n_1}Q_{mn}^{m_1n_1}}{\left(\alpha_m^2+\beta_n^2\right)\left(\alpha_{m_1}^2+\beta_{n_1}^2\right)}\sin(\alpha_m y_1)\\
& \cdot\sin(\beta_n y_2)\sin(\alpha_{m_1}x_1)\sin\left(\beta_{n_1}x_2\right).
\end{aligned}
\tag{37}
$$

The velocity covariance can be readily formulated from a simple relationship $u_{ij}(\mathbf{x}, t; \mathbf{y}, \tau) = q_{ij}(\mathbf{x}, t; \mathbf{y}, \tau)/\phi(\mathbf{x})/\phi(\mathbf{y})$, where ϕ is the porosity of the porous media and is considered as a deterministic quantity due to its relatively small variability.

3. Numerical Examples

[15] In this section, we try to examine the convergence and the accuracy of the analytical solutions for the first-order transient mean flow quantities and related (cross) covariances. We consider a two-dimensional rectangular domain in a saturated heterogeneous porous medium. The flow domain for our base case is a square of a size $L_1 = L_2 = 10$ (in any consistent length unit), uniformly discretized into 40×40 square elements. The no-flow conditions are prescribed at two lateral boundaries and constant heads are specified on the left and right boundaries. Initially, the flow is at steady state with constant heads $H_{10} = 9.5$ on the left boundary and $H_{20} = 9.0$ on the right boundary. At time $t = 0$, the constant heads on the left and right boundaries are suddenly changed to $H_1 = 11.0$ and $H_2 = 10.0$, respectively. The storativity is a deterministic constant $S = 0.005$. The mean of the log transmissivity is given as $\langle Y \rangle = 0.0$ (i.e., the geometric mean of transmissivity $T_G = 1.0$). The variance and the correlation lengths of the log transmissivity field for our base case are $\sigma_Y^2 = 1.0$ and $\lambda_1 = \lambda_2 = 1.0$. Unless specifically mentioned, in all examples we will show results only along the profile $x_2 = L_2/2 = 5$.

3.1. Convergence of Analytical Solutions

[16] An important aspect of analytical solutions presented as infinity series is how fast the solutions converge to their true solutions, or in other words, how many terms should be included in truncating the series so that the approximations to these solutions will have a given accuracy. Many factors, including the aspect ratio of the flow domain and the correlation lengths of the log transmissivity field, may impact the rate of convergence. To investigate this, in addition to the base case, we design two more cases. For each case, we truncate each individual summation (each index) in the analytical solutions to the mean head and the head variance after N terms, where $N = 2$, 3, 5, 6, and 10. Figure 1 illustrates the computed transient mean head at four times $t = 0.0$, 0.01, 0.05, and 0.4, using $N = 2$, 3, and 5. The figure shows that at time $t = 0.4$, the flow has reached the final steady state. From the figure we see that keeping the first two terms in the summation of $h^{(0)}(\mathbf{x})$ is very accurate, except for at early time $t = 0.01$, in which keeping the first three terms is accurate enough. In all examples presented in this study, approximating the mean head with the first three terms in (7) is sufficiently accurate, and adding more terms does not significantly improve the accuracy. Mathematical analysis of the expression for $h^{(0)}(\mathbf{x})$, i.e., (7), reveals that for an extremely small t, a very large number of terms is needed. However, in general, the series in (7) converges very fast, and therefore, we will focus our discussion on the head variance. Figure 2 depicts the head variance as a function of x_1 along the profile $x_2 = L_2/2$ for different values of N. The figure clearly demonstrates that the rate of convergence depends on the flow condition. When the flow is close to steady state, for instance at $t = 0.4$, approximating the head variance using $N = 3$ (i.e., 729 terms in a sixfold summation) will be very accurate. While at early times, due to the sudden change on constant head boundary at $t = 0$, more terms are needed to approximate the head variance.

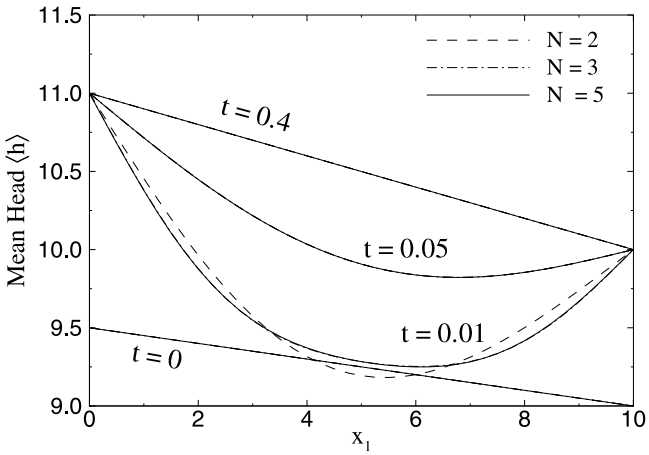

Figure 1. Transient mean head computed using different numbers of terms, N, in truncating infinite series in (7): the base case.

[17] To examine the possible effect of the domain geometry (the ratio L_1/L_2) on the convergence of the solution, we change the width of the domain to $L_2 = 2$ while keeping everything else the same as in the base case. Numerical experiments with different numbers of terms included in the truncated summations are illustrated in Figure 3, which depicts the mean head and head variance along the profile $x_2 = L_2/2 = 1.0$. The figure, again, shows that the analytical solution converges faster when the flow is at or near steady state. In addition, comparing Figures 2 and 3, one finds that the head variance increases as the domain becomes narrower in the transverse direction.

[18] In the third example, we increase the correlation lengths of the log transmissivity to $\lambda_1 = \lambda_2 = 5$. The results, as shown in Figure 4, indicate that an increase of the correlation length enhances the rate of convergence of the analytical solution (compared to Figure 2).

3.2. Accuracy of Analytical Solutions

[19] We conduct Monte Carlo (MC) simulations to verify the accuracy of the first-order analytical solutions for transient head and its related (cross) covariances. First, we generate 5,000 two-dimensional unconditional realizations of the log transmissivity with the separable covariance function as given in (16), using the random field generator based on the Karhunen-Loève decomposition, as described by *Zhang and Lu* [2004]. The quality of these realizations has been examined by comparing their sample statistics (mean, variance, and correlation lengths) with the specified mean and covariance functions. The comparisons show that the generated random fields reproduce the specified mean and covariance functions very well.

[20] For each realization, we solve the steady state flow equation with the initial constant head $H_{10} = 9.5$ and $H_{20} = 9.0$ on the left and the right boundaries, using the finite element heat and mass transfer code (FEHM) of *Zyvoloski et al.* [1997]. This steady state head field is then taken as the

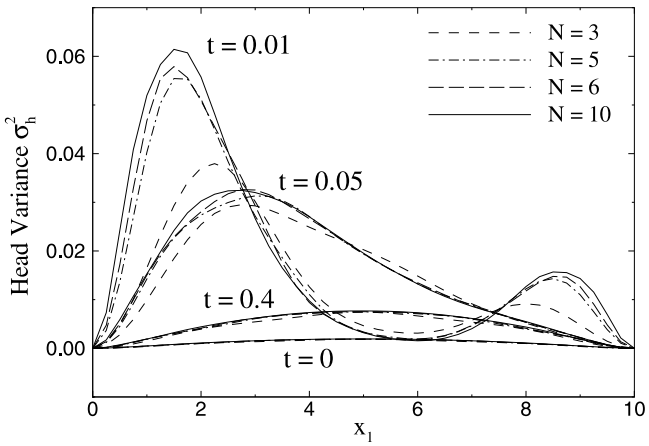

Figure 2. Transient head variance computed using different numbers of terms, *N*, in truncating infinite series in (22): the base case.

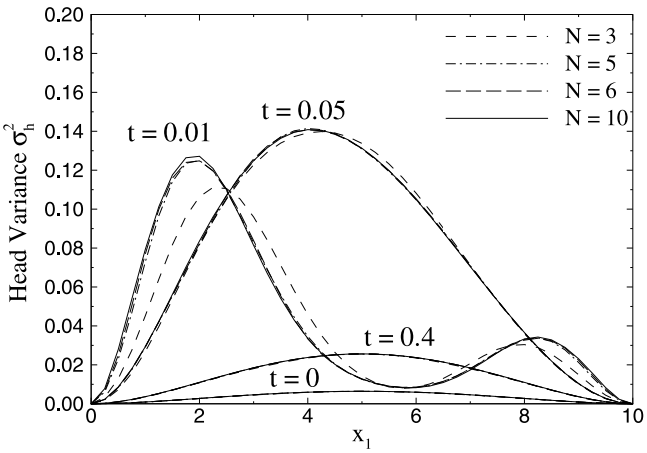

Figure 4. Transient head variance computed using different numbers of terms in truncating infinite series in (22): $\lambda_1 = \lambda_2 = 5.0$.

initial head $H_0(\mathbf{x})$ for the following transient simulation. Using the same realization, we run the FEHM code again for a transient simulation with the new constant heads H_1 = 11.0 and H_2 = 10.0 on the left and right boundaries and record the head at the following times: t = 0, 0.01, 0.05, and 0.4. This procedure is repeated for all realizations, and the sample statistics of the transient flow fields, i.e., the mean predictions of the head and the flux as well as their (cross) covariances at these times, are computed from realizations. These flow statistics are considered the "true" solutions that are used to evaluate the accuracy of the first-order analytical solutions.

[21] Figure 5a compares the transient mean head $\langle h(\mathbf{x}, t)\rangle$ computed from Monte Carlo simulations (MC, solid curves) and that from the first-order (in σ_Y) analytical solution with N = 10 (ANA, dashed curves) at various times along the profile $x_2 = L_2/2$. It seems from the figure that the mean head computed from the analytical solution is very close to the Monte Carlo results, especially at or near steady state. Also compared in the figure is the first-order mean head computed from the moment equation method (ME, dash-dotted curves) [*Zhang and Lu*, 2004], where the input covariance function for the ME method is the analytical expression (16). Figure 5b compares the transient head variance obtained from the MC simulations, the first-order analytical solution, and the first-order ME approach at various times. It is expected that the first-order analytical solutions should be identical to the results from the first-order ME method, in the limit that the number of terms, *N*, in the truncated finite series of the analytical solutions approaches infinity. Furthermore, both first-order results will deviate slightly from the Monte Carlo results, and such deviations will increase with the increase of the variability of the log transmissivity. Figure 5 clearly shows that the analytical solutions are adequately accurate at σ_Y^2 = 1.0, especially when the flow is at or near steady state.

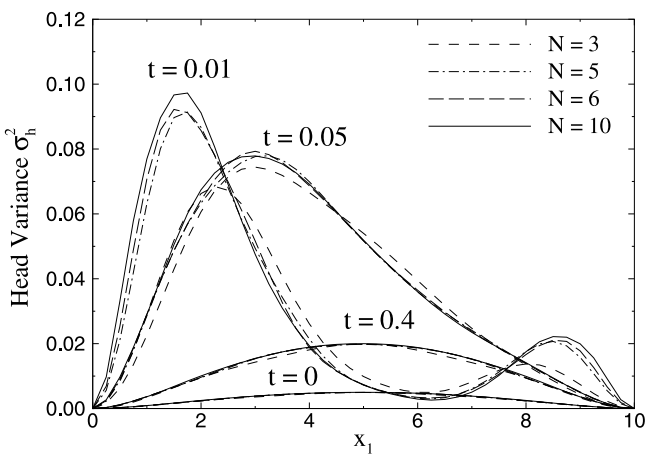

Figure 3. Transient head variance computed using different numbers of terms in truncating infinite series in (22): L_2= 2.0.

[22] It is interesting to see from Figure 5b that the head variance along the profile $x_2 = L_2/2$ at both the initial and final steady state is symmetric (larger head variance at the final steady state due to a larger hydraulic gradient), while at any unsteady state the curve is asymmetric. For example, the head variance along the profile has two peaks at time t = 0.01. This may be due to the variable hydraulic gradient during the unsteady state. Comparison of Figures 5a and 5b indicates that the larger peak on the variance curve corresponds to a larger hydraulic gradient on the mean head curve. Furthermore, because the change of the head variance from the initial head variance is due to the change of constant head boundaries at t = 0, the variance change starts from two constant head boundaries and propagates into the entire flow domain. As a result, at a time before the effect of the boundary change reaches the entire domain, the head variance in some region remains the same as the initial head variance $\sigma_{H0}^2(\mathbf{x})$ (e.g., a trough at t = 0.01 in Figure 5b).

[23] We should emphasize here that in our comparisons, it is assumed that the results from Monte Carlo simulations are accurate. It is possible to estimate the bounds of errors around the Monte Carlo results, using the procedure proposed by *Ballio and Guadagnini* [2004]. For example, given the number of realizations and a confidence level of 95%, the true head variance σ_h^2 should satisfy the following relationship: $0.962S_n^2 \le \sigma_h^2 \le 1.0406S_n^2$, where S_n^2 is the sample variance of head from Monte Carlo simulations.

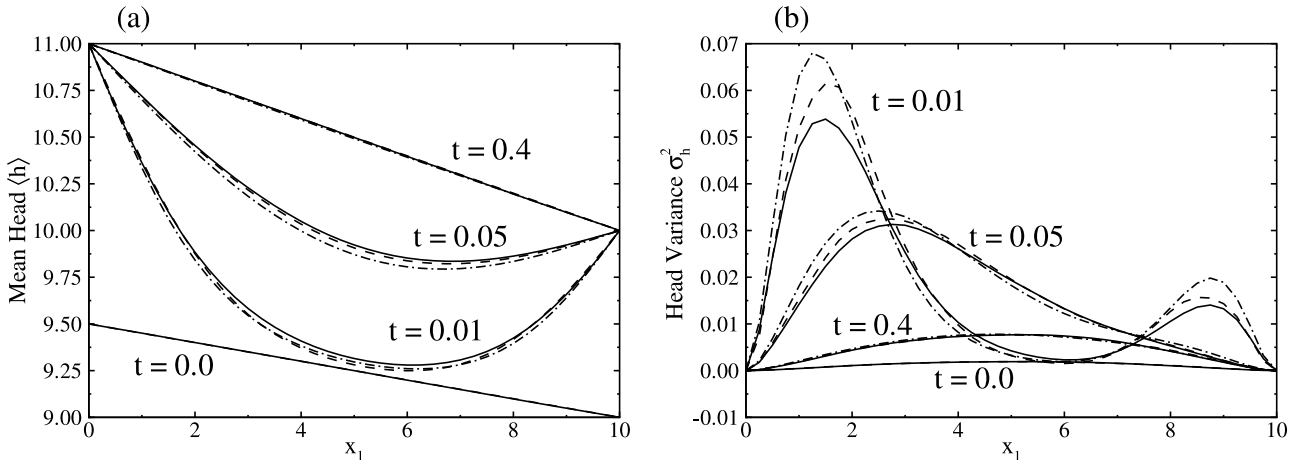

Figure 5. Comparisons of (a) the transient mean head and (b) the transient head variance computed from Monte Carlo simulations (solid curves), the first-order analytical solution (dashed curves), and the first-order moment equation method (dash-dotted curves).

[24] Figure 6a illustrates the cross covariance $C_{Yh}(\mathbf{x}; \mathbf{x}, t)$ as a function of x_1 obtained from Monte Carlo simulations (solid curves) and analytical solutions (dashed curves) at four elapsed times. It is evident that analytical results are in good agreement with Monte Carlo results. Note that, at early time, $C_{Yh}(\mathbf{x}; \mathbf{x}, t)$ is much larger than its values at steady state. This implies that at early time, the effect of the transmissivity is relatively local, i.e., the transmissivity at point $\mathbf{x}$ has a significant effect on the mean head at the same point $\mathbf{x}$. Such an effect reduces significantly at later times because the transmissivity elsewhere in the domain also impact the mean head at point $\mathbf{x}$.

[25] Figure 6b depicts the cross covariance between the log transmissivity at the center of domain ($L_1/2$, $L_2/2$) and the head $h(\mathbf{x}, t)$ along the profile $x_2 = L_2/2$, as a function of x_1. Again, analytical results are in good agreement with Monte Carlo results. It is interesting to note that, at both the initial and the final steady state, C_{Yh} along this profile is antisymmetric and $C_{Yh} = 0$ for Y and $h(\mathbf{x}, t)$ at the center of the domain, due to the particular boundary conditions in our problem. However, at any transient state, C_{Yh} does not shown any such kind of symmetry.

[26] Figure 7 shows the covariance of head at (x_1, $L_2/2$, t) and (x_1, $L_2/2$, τ) as a function of x_1 and τ at two different times $t = 0.00$ and $t = 0.05$, where solid curves stand for the results from Monte Carlo simulations and dashed curves from analytical solutions. Note that the head covariance function between two steady states ($t = 0.0$ and $\tau = 0.0$, or $t = 0.0$ and $\tau = 0.4$) along the central line of the domain is symmetric (see the curves for $\tau = 0.0$ and $\tau = 0.4$ in Figure 7a). The difference between these two curves is due to the difference in the magnitude of the hydraulic gradient. At unsteady state, the pattern of the head covariance function depends on the spatial locations and elapsed time.

[27] Comparisons of the mean longitudinal flux obtained from the MC simulations, the analytical solution, and the ME method are illustrated in Figure 8, and similar comparisons for the flux variance are depicted in Figure 9, where the plots for a later time $t = 0.4$ are enlarged in inserts for a detail view. Clearly, Figures 8–9 once again demonstrate

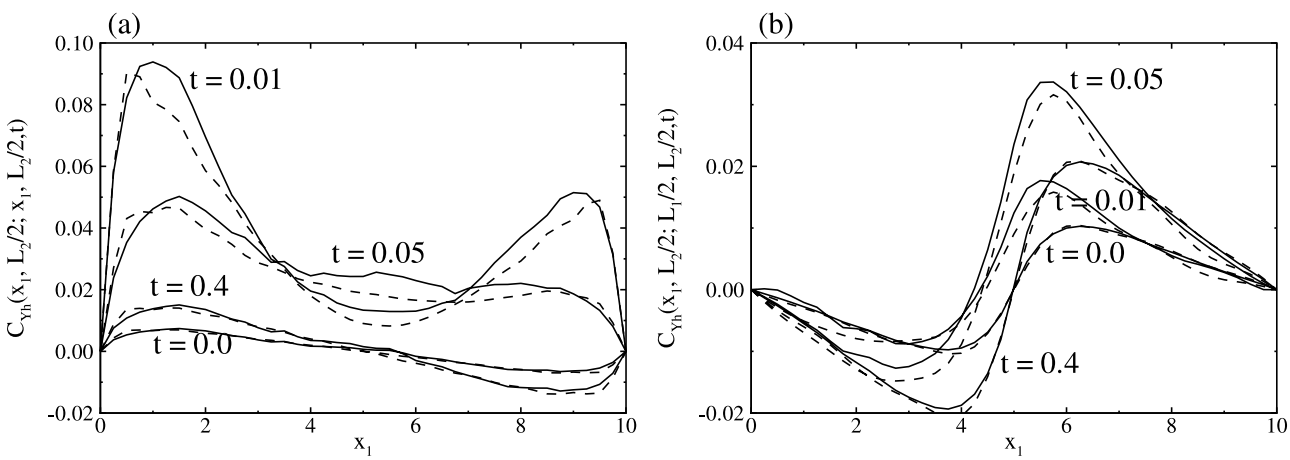

Figure 6. Transient cross-covariance (a) between the log transmissivity $Y(x_1, L_2/2)$ and the hydraulic head $h(x_1, L_2/2, t)$ and (b) between the log transmissivity $Y(L_1/2, L_2/2)$ and the hydraulic head $h(x_1, L_2/2, t)$.

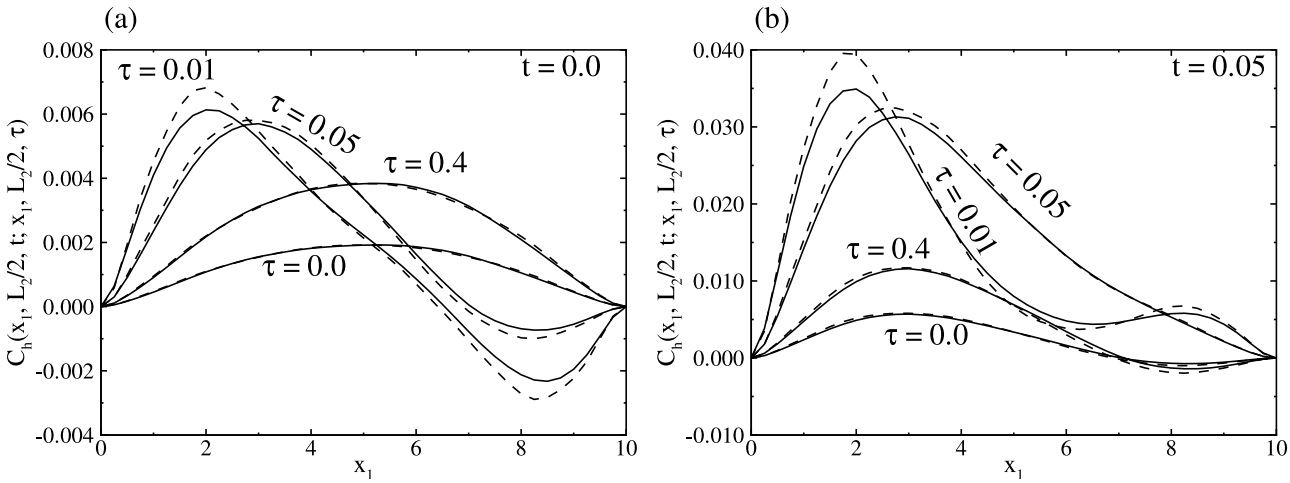

Figure 7. Transient head covariance between head $h(\mathbf{x}, t)$ and $h(\mathbf{x},\tau)$ as a function of x_1 and time τ along $x_2 = L_2/2$ for (a) $t = 0.0$ and (b) $t = 0.05$.

the accuracy of the analytical solutions. In addition, the transient flux variance could be significantly larger than the steady state counterpart.

4. Conclusions

[28] This study leads to the following conclusions.

[29] 1. Statistical moments for transient flow in two-dimensional bounded randomly heterogeneous media are amenable to analytical solutions. We derive analytical solutions to the moments (mean and covariance of both the hydraulic head and the flux) for transient saturated flow in two-dimensional bounded, randomly heterogeneous porous media, assuming that the flow is initially at steady state. More specifically, we first obtain partial differential equations governing the zeroth-order head $h^{(0)}$ and the first-order head term $h^{(1)}$, using perturbation expansions. We then solve $h^{(0)}$ and $h^{(1)}$ analytically. The head perturbation $h^{(1)}$ is used to derive expressions for autocovariance of the hydraulic head and the cross covariance between the log transmissivity and the head. Upon solving for the head moments, the expressions for the mean flux and flux covariance tensor are formulated based on Darcy's law. These solutions are presented as infinite series.

[30] 2. Numerical experiments have been conducted to evaluate the convergence of these analytical solutions. It has been shown that the rate of convergence depends on the flow condition, the aspect ratio of the flow domain (L_1/L_2), and the correlation lengths of the transmissivity. When the flow is at or near steady state, the analytical solutions converge very fast, and for unsteady flow, more terms in the truncated finite series are required to approximate the statistical moments. In addition, a large aspect ratio enhances the rate of convergence. Furthermore, large correlation lengths lead to fast convergence. Finally, the solutions for the mean quantities converge faster than do the solutions for the second moments.

[31] 3. The accuracy of these first-order analytical solutions has been examined by comparing them with solutions from both Monte Carlo simulations and the numerical moment equation method. The numerical experiments clearly show that the first-order analytical solutions are adequately accurate at least for $\sigma_Y^2 = 1.0$.

[32] 4. The initial steady state uncertainty on the head in this study is determined rather than arbitrarily prescribed, under the assumption that the variability of the log permeability is the only source of uncertainty. This allows us to apply the analytical solutions recursively if needed (e.g., owing to changes on boundary conditions): the solved steady state solutions can be further taken as the initial condition to predict responses of flow moments due to such changes.

Appendix A: Zeroth-Order Mean Head $h^{(0)}(\mathbf{x}, t)$

[33] Here we briefly outline the procedure for solving the following equation for the zeroth-order mean head $h^{(0)}(\mathbf{x}, t)$:

$$\frac{\partial^2 h^{(0)}(\mathbf{x},t)}{\partial x_1^2} + \frac{\partial^2 h^{(0)}(\mathbf{x},t)}{\partial x_2^2} = \frac{S}{T_G}\frac{\partial h^{(0)}(\mathbf{x},t)}{\partial t}, \qquad \text{(A1)}$$

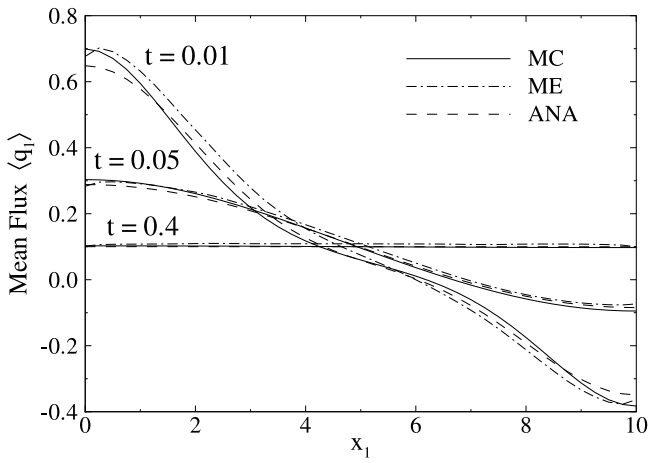

Figure 8. Comparisons of the transient mean longitudinal flux computed from Monte Carlo simulations (solid curves), the first-order analytical solution (dashed curves), and the first-order moment equation method (dash-dotted curves).

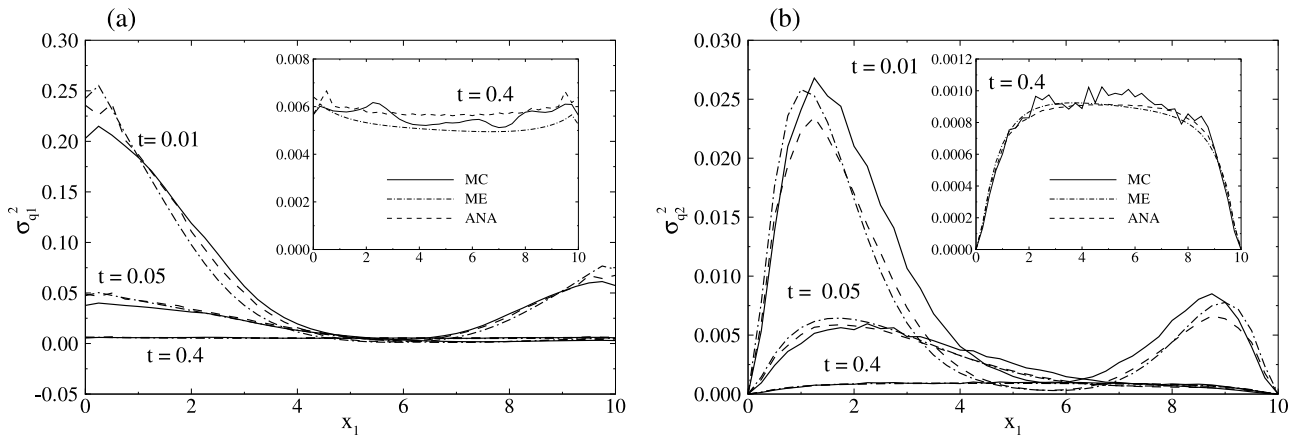

Figure 9. Comparisons of (a) the longitudinal flux variance and (b) the transverse flux variance computed from Monte Carlo simulations (solid curves), the first-order analytical solution (dashed curves), and the first-order moment equation method (dash-dotted curves).

with boundary conditions and initial conditions as shown in (5a)–(5e). Under the given boundary conditions, by using an integral transformation [*Özişik*, 1989],

$$h^*(\alpha_m,\beta_n,t)=\int_\Omega K(\alpha_m,x_1)\,K(\beta_n,x_2)\,h^{(0)}(\mathbf{x},t)\,d\,\mathbf{x}, \tag{A2}$$

where kernels

$$K(\alpha_m,x_1)=\sqrt{\frac{2}{L_1}}\sin(\alpha_m x_1), \tag{A3}$$

$$K(\beta_n,x_2)=\begin{cases}\sqrt{\dfrac{2}{L_2}}\cos(\beta_n x_2) & \text{if } n\neq 0,\\ \sqrt{\dfrac{1}{L_2}} & \text{if } n=0,\end{cases}, \tag{A4}$$

and $\alpha_m = m\pi/L_1$, $m = 1, 2, \cdots$, $\beta_n = n\pi/L_2$, $n = 0, 1, \cdots$, (A1) is transformed to a first-order ordinary differential equation,

$$\frac{dh^*(\alpha_m,\beta_n,t)}{dt}+\frac{T_G}{S}\left(\alpha_m^2+\beta_n^2\right)h^*(\alpha_m,\beta_n,t)=A(\alpha_m,\beta_n,t), \tag{A5}$$

with the initial condition

$$F^*(\alpha_m,\beta_n)=\int_\Omega K(\alpha_m,x_1)\,K(\beta_n,x_2)\,\langle H_0(\mathbf{x})\rangle\,d\mathbf{x}, \tag{A6}$$

which is the transformation of the initial condition (5e). It should be noted that the integral transformation presented in (A2)–(A4) can be considered as the Fourier transformation in the two-dimensional space, by which the partial differential equation (A1) is transformed into an ordinary differential equation of the Fourier coefficients, i.e., (A5). The term on the right-hand side of (A5) is related to boundary conditions of the original zeroth-order equation:

$$\begin{aligned}A(\alpha_m,\beta_n,t)=&\frac{T_G}{S}\left[\left.\frac{dK(\alpha_m,x_1)}{dx_1}\right|_{x_1=0}\int_{x_2=0}^{L_2}K(\beta_n,x_2)H_1\,dx_2\right.\\&\left.+\left.\frac{dK(\alpha_m,x_1)}{dx_1}\right|_{x_1=L_1}\int_{x_2=0}^{L_2}K(\beta_n,x_2)H_2\,dx_2\right]\\=&\begin{cases}0 & \text{if } n\neq 0,\\ \dfrac{T_G}{S}\sqrt{\dfrac{2L_2}{L_1}}\alpha_m(H_1-(-1)^mH_2) & \text{if } n=0,\end{cases}.\end{aligned} \tag{A7}$$

Equation (A5) with the initial condition (A6) can be solved easily:

$$h^*(\alpha_m,\beta_n,t)=F^*(\alpha_m,\beta_n)+\int_{t'=0}^{t}e^{\frac{T_G}{S}\left(\alpha_m^2+\beta_n^2\right)t'}A(\alpha_m,\beta_n,t')dt', \tag{A8}$$

and the solution for $h^{(0)}(\mathbf{x}, t)$ can be derived from back transformation of $h^*(\alpha_m, \beta_n, t)$:

$$\begin{aligned}h^{(0)}(\mathbf{x},t)=&\sum_{m=1}^{\infty}\sum_{n=0}^{\infty}e^{-\frac{T_G}{S}\left(\alpha_m^2+\beta_n^2\right)t}K(\alpha_m,x_1)K(\beta_n,x_2)h^*(\alpha_m,\beta_n,t)\\=&\sum_{m=1}^{\infty}\sum_{n=0}^{\infty}e^{-\frac{T_G}{S}\left(\alpha_m^2+\beta_n^2\right)t}K(\alpha_m,x_1)K(\beta_n,x_2)\int_\Omega K\left(\alpha_m,x_1'\right)\\&\cdot K\left(\beta_n,x_2'\right)\langle H_0(\mathbf{x}')\rangle\,d\mathbf{x}'+\frac{2}{L_1}\sum_{m=1}^{\infty}\frac{\sin(\alpha_m x_1)}{\alpha_m}\\&\cdot\left(H_1-(-1)^mH_2\right)\left(1-e^{-\frac{T_G}{S}\alpha_m^2t}\right).\end{aligned} \tag{A9}$$

Assuming $\langle H_0(\mathbf{x})\rangle = H_{10} + (H_{20} - H_{10})\,x_1/L_1$, (A9) reduces to

$$\begin{aligned}h^{(0)}(\mathbf{x},t)=&\frac{2}{L_1}\sum_{m=1}^{\infty}\frac{\sin(\alpha_m x_1)}{\alpha_m}\left[(H_{10}-(-1)^mH_{20})e^{-\frac{T_G}{S}\alpha_m^2t}\right.\\&\left.+\left(H_1-(-1)^mH_2\right)\left(1-e^{-\frac{T_G}{S}\alpha_m^2t}\right)\right].\end{aligned} \tag{A10}$$

For boundary conditions other than those shown in (5a)–(5d), transformations similar to (A2) can be used upon replacing with appropriate kernels [*Özişik*, 1989].

Appendix B: Head Perturbation $h'(\mathbf{x}, t)$

[34] Perturbation term $h^{(1)}(\mathbf{x}, t)$ reads as

$$\frac{\partial^2h^{(1)}(\mathbf{x},t)}{\partial x_i^2}+\frac{\partial}{\partial x_i}\left(Y'(\mathbf{x})\frac{\partial h^{(0)}(\mathbf{x},t)}{\partial x_i}\right)=\frac{S}{T_G}\frac{\partial h^{(1)}(\mathbf{x},t)}{\partial t}, \tag{B1}$$

with boundary conditions and initial conditions as shown in (11). Similarly, using an integral transformation [*Özişik*, 1989],

$$h^*(\alpha_m,\beta_n,t)=\int_\Omega K(\alpha_m,x_1)\,K(\beta_n,x_2)\,h^{(1)}(\mathbf{x},t)\,d\,\mathbf{x}, \tag{B2}$$

where kernels are given in (A3)–(A4), (B1) is transformed to a first-order ordinary differential equation,

$$\frac{dh^*(\alpha_m,\beta_n,t)}{dt}+\frac{T_G}{S}\left(\alpha_m^2+\beta_n^2\right)h^*(\alpha_m,\beta_n,t)=A(\alpha_m,\beta_n,t), \quad \text{(B3)}$$

with the initial condition $F^*(\alpha_m, \beta_n) = \int_\Omega K(\alpha_m, x_1)K(\beta_n, x_2)H_0'(\mathbf{x})d\mathbf{x}$. The solution to (B3) can be formally expressed as

$$h^*(\alpha_m,\beta_n,t)=F^*(\alpha_m,\beta_n)+\int_{t'=0}^{t} e^{\frac{T_G}{S}\left(\alpha_m^2+\beta_n^2\right)t'}A(\alpha_m,\beta_n,t')dt', \quad \text{(B4)}$$

and the solution for $h^{(1)}(\mathbf{x}, t)$ can be derived from the back transformation of $h^*(\alpha_m, \beta_n, t)$:

$$h^{(1)}(\mathbf{x},t)=\sum_{m=1}^{\infty}\sum_{n=0}^{\infty}e^{-\frac{T_G}{S}\left(\alpha_m^2+\beta_n^2\right)t}K(\alpha_m,x_1)K(\beta_n,x_2)h^*(\alpha_m,\beta_n,t). \quad \text{(B5)}$$

[35] The term on the right-hand side of (B3) is related to boundary conditions for $h^{(1)}$ and the source term, i.e., the second term on the left-hand side of (B1):

$$A(\alpha_m,\beta_n,t)=\frac{T_G}{S}\int_\Omega K(\alpha_m,x_1)\,K(\beta_n,x_2)\frac{\partial}{\partial x_i}\left(Y'(\mathbf{x})\frac{\partial h^{(0)}(\mathbf{x},t)}{\partial x_i}\right)\cdot d\,\mathbf{x}. \quad \text{(B6)}$$

Substituting $h^{(0)}(\mathbf{x}, t)$ into (B6) and carrying out integration yields

$$A(\alpha_m,\beta_n,t)=\frac{2J_1T_G\alpha_m}{\sqrt{L_1L_2}S}\int_\Omega Y'(\mathbf{x}')\cos\left(\alpha_m x_1'\right)\cos\left(\beta_n x_2'\right)d\mathbf{x}' - \frac{4T_G\alpha_m}{L_1\sqrt{L_1L_2}S}\sum_{k=1}^{\infty}b_k e^{-\frac{T_G}{S}\alpha_k^2 t}\int_\Omega Y'(\mathbf{x}')\cos\left(\alpha_m x_1'\right)\cdot\cos\left(\alpha_k x_1'\right)\cos\left(\beta_n x_2'\right)d\mathbf{x}' \quad \text{(B7)}$$

for $n \neq 0$ and

$$A(\alpha_m,\beta_0,t)=\frac{\sqrt{2}J_1T_G\alpha_m}{\sqrt{L_1L_2}S}\int_\Omega Y'(\mathbf{x}')\cos\left(\alpha_m x_1'\right)d\mathbf{x}'-\frac{2\sqrt{2}T_G\alpha_m}{L_1\sqrt{L_1L_2}S}\cdot\sum_{k=1}^{\infty}b_k e^{-\frac{T_G}{S}\alpha_k^2 t}\int_\Omega Y'(\mathbf{x}')\cos\left(\alpha_m x_1'\right)\cos\left(\alpha_k x_1'\right)d\mathbf{x}', \quad \text{(B8)}$$

for $n = 0$. Substituting $A(\alpha_m, \beta_n, t)$ and $F^*(\alpha_m, \beta_n)$ into (B4) and combining the latter with (B5), one obtains the solution for $h^{(1)}(\mathbf{x}, t)$:

$$\begin{aligned}h^{(1)}(\mathbf{x},t)=&\frac{4}{D}\sum_{\substack{m=1\\n=0}}^{\infty}a_n\sin(\alpha_m x_1)\cos(\beta_n x_2)e^{-\frac{T_G}{S}\left(\alpha_m^2+\beta_n^2\right)t}\int_\Omega H_0'(\mathbf{x}')\\&\cdot\sin\left(\alpha_m x_1'\right)\cos\left(\beta_n x_2'\right)d\mathbf{x}'+\frac{4J_1}{D}\sum_{\substack{m=1\\n=0}}^{\infty}\\&\cdot\frac{a_n\alpha_m\sin(\alpha_m x_1)\cos(\beta_n x_2)}{\alpha_m^2+\beta_n^2}\left[1-e^{-\frac{T_G}{S}\left(\alpha_m^2+\beta_n^2\right)t}\right]\int_\Omega Y'(\mathbf{x}')\\&\cdot\cos\left(\alpha_m x_1'\right)\cos\left(\beta_n x_2'\right)d\mathbf{x}'-\frac{8T_G}{DL_1S}\sum_{\substack{m,k=1\\n=0}}^{\infty}\\&\cdot a_n b_k P_{kmn}(t)\alpha_m\sin(\alpha_m x_1)\cos(\beta_n x_2)\int_\Omega Y'(\mathbf{x}')\cos\\&\cdot\left(\alpha_m x_1'\right)\cos\left(\alpha_k x_1'\right)\cos\left(\beta_n x_2'\right)d\mathbf{x}',\end{aligned} \quad \text{(B9)}$$

where $D = L_1L_2$, $a_n = 1$ for $n \geq 1$ and $a_n = 1/2$ for $n = 0$ and

$$P_{kmn}(t)=\begin{cases}\frac{S}{T_G}\frac{e^{-\frac{T_G}{S}\alpha_k^2 t}-e^{-\frac{T_G}{S}\left(\alpha_m^2+\beta_n^2\right)t}}{\alpha_m^2+\beta_n^2-\alpha_k^2}, & \text{if } \alpha_k^2\neq\alpha_m^2+\beta_n^2,\\ t\,e^{-\frac{T_G}{S}\left(\alpha_m^2+\beta_n^2\right)t}, & \text{if } \alpha_k^2=\alpha_m^2+\beta_n^2.\end{cases} \quad \text{(B10)}$$

The steady state solution of the head perturbation can be derived by taking the limit of (B9) as $t \to \infty$:

$$h^{(1)}(\mathbf{x},\infty)=\frac{4J_1}{D}\sum_{\substack{m=1\\n=0}}^{\infty}\frac{a_n\alpha_m\sin(\alpha_m x_1)\cos(\beta_n x_2)}{\alpha_m^2+\beta_n^2}\int_\Omega Y'(\mathbf{x}')\cos\cdot\left(\alpha_m x_1'\right)\cos\left(\beta_n x_2'\right)d\mathbf{x}'. \quad \text{(B11)}$$

Appendix C: Head Covariance

[36] Equation (B9) and taking ensemble mean yields an expression for head covariance:

$$\begin{aligned}C_h(\mathbf{x},t;\mathbf{y},\tau)=&\left\langle h^{(1)}(\mathbf{x},t)\,h^{(1)}(\mathbf{y},\tau)\right\rangle\\=&\frac{4}{D}\sum_{\substack{m=1\\n=0}}^{\infty}a_n\sin(\alpha_m x_1)\cos(\beta_n x_2)e^{-\frac{T_G}{S}\left(\alpha_m^2+\beta_n^2\right)t}\int_\Omega\\&\cdot\left\langle H_0'(\mathbf{x}')h^{(1)}(\mathbf{y},\tau)\right\rangle\sin\left(\alpha_m x_1'\right)\cos\left(\beta_n x_2'\right)d\mathbf{x}'\\&+\frac{4J_1}{D}\sum_{\substack{m=1\\n=0}}^{\infty}\frac{a_n\alpha_m\sin(\alpha_m x_1)\cos(\beta_n x_2)}{\alpha_m^2+\beta_n^2}\\&\cdot\left[1-e^{-\frac{T_G}{S}\left(\alpha_m^2+\beta_n^2\right)t}\right]\int_\Omega C_{Yh}(\mathbf{x}';\mathbf{y},\tau)\cos\left(\alpha_m x_1'\right)\\&\cdot\cos\left(\beta_n x_2'\right)d\mathbf{x}'-\frac{8T_G}{DL_1S}\sum_{\substack{m,k=1\\n=0}}^{\infty}a_n b_k P_{kmn}(t)\alpha_m\\&\cdot\sin(\alpha_m x_1)\cos(\beta_n x_2)\int_\Omega C_{Yh}(\mathbf{x}';\mathbf{y},\tau)\\&\cdot\cos\left(\alpha_m x_1'\right)\cos\left(\alpha_k x_1'\right)\cos\left(\beta_n x_2'\right)d\mathbf{x}'.\end{aligned} \quad \text{(C1)}$$

Here the cross covariance between head at space-time $(\mathbf{y}, \tau)$ and initial head at location $\mathbf{x}$, $\langle H_0'(\mathbf{x})h^{(1)}(\mathbf{y}, \tau)\rangle$, can be derived by rewriting (B9) in terms of $(\mathbf{y}, \tau)$, multiplying $H_0'(\mathbf{x}')$ to the derived equation, and taking the mean:

$$\begin{aligned}C_{H_0h}(\mathbf{x};\mathbf{y},\tau)=&\left\langle H_0(\mathbf{x})\,h^{(1)}(\mathbf{y},\tau)\right\rangle\\=&\frac{4}{D}\sum_{\substack{m=1\\n=0}}^{\infty}a_n\sin(\alpha_m y_1)\cos(\beta_n y_2)e^{-\frac{T_G}{S}\left(\alpha_m^2+\beta_n^2\right)\tau}\int_\Omega\\&\cdot C_{H_0}(\mathbf{x}',\mathbf{x})\sin\left(\alpha_m x_1'\right)\cos\left(\beta_n x_2'\right)d\mathbf{x}'+\frac{4J_1}{D}\sum_{\substack{m=1\\n=0}}^{\infty}\\&\cdot\frac{a_n\alpha_m\sin(\alpha_m y_1)\cos(\beta_n y_2)}{\alpha_m^2+\beta_n^2}\left[1-e^{-\frac{T_G}{S}\left(\alpha_m^2+\beta_n^2\right)\tau}\right]\int_\Omega\\&\cdot C_{YH_0}(\mathbf{x}',\mathbf{x})\cos\left(\alpha_m x_1'\right)\cos\left(\beta_n x_2'\right)d\mathbf{x}'-\frac{8T_G}{DL_1S}\\&\cdot\sum_{\substack{m,k=1\\n=0}}^{\infty}a_n b_k P_{kmn}(\tau)\alpha_m\sin(\alpha_m y_1)\cos(\beta_n y_2)\int_\Omega\\&\cdot C_{YH_0}(\mathbf{x}',\mathbf{x})\cos\left(\alpha_m x_1'\right)\cos\left(\alpha_k x_1'\right)\cos\left(\beta_n x_2'\right)d\mathbf{x}'.\end{aligned} \quad \text{(C2)}$$

As mentioned early, we assume that the flow is initially at steady state and the perturbation of the initial head $H_0'(x)$ is

determined from the steady state condition. Therefore $C_{YH_0}(\mathbf{x}', \mathbf{x})$ and $C_{H_0}(\mathbf{x}', \mathbf{x})$ can be obtained by replacing J_1 in (15) and (18) by J_0, the initial hydraulic gradient. Substituting C_{YH_0} and C_{H_0} into (C2) and carrying out integrations, one has

$$C_{H_0h}(\mathbf{x};\mathbf{y},\tau) = \langle H_0(\mathbf{x})\, h^{(1)}(\mathbf{y},\tau)\rangle = \frac{16J_0}{D^2}\sum_{\substack{m,m_1=1\\ n,n_1=0}}^{\infty}\frac{a_n a_{n_1}\alpha_m\alpha_{m_1}Q^{mn}_{m_1n_1}SC}{\left(\alpha_m^2+\beta_n^2\right)\left(\alpha_{m_1}^2+\beta_{n_1}^2\right)}J_{mn}(\tau) - \frac{32J_0T_G}{D^2L_1S}\sum_{\substack{m,m_1,k=1\\ n,n_1=0}}^{\infty}\frac{a_n a_{n_1}b_k P_{kmn}(\tau)\alpha_m\alpha_{m_1}Q^{kmn}_{m_1n_1}SC}{\left(\alpha_{m_1}^2+\beta_{n_1}^2\right)}, \tag{C3}$$

where

$$SC = \sin(\alpha_m y_1)\cos(\beta_n y_2)\sin(\alpha_{m_1}x_1)\cos\left(\beta_{n_1}x_2\right), \tag{C4}$$

$$J_{mn}(\tau) = \left[J_1 + (J_0 - J_1)e^{-\frac{T_G}{S}\left(\alpha_m^2+\beta_n^2\right)\tau}\right], \tag{C5}$$

$$R_{m_1n_1}(\mathbf{x}) = \int_\Omega C_Y(\mathbf{x},\mathbf{x}')\cos\left(\alpha_{m_1}x_1'\right)\cos\left(\beta_{n_1}x_2'\right)d\mathbf{x}' = \frac{\lambda_1\lambda_2\sigma_Y^2}{\left(\alpha_{m_1}^2\lambda_1^2+1\right)\left(\beta_{n_1}^2\lambda_2^2+1\right)} \cdot\left[2\cos(\alpha_{m_1}x_1) - e^{-x_1/\lambda_1} - (-1)^{m_1}e^{(x_1-L_1)/\lambda_1}\right] \cdot\left[2\cos\left(\beta_{n_1}x_2\right) - e^{-x_2/\lambda_2} - (-1)^{n_1}e^{(x_2-L_2)/\lambda_2}\right], \tag{C6}$$

$$Q^{mn}_{m_1n_1} = \int_\Omega R_{m_1n_1}(\mathbf{x})\cos(\alpha_m x_1)\cos(\beta_n x_2)d\mathbf{x} = \frac{\lambda_1\lambda_2\sigma_Y^2}{\left(\alpha_{m_1}^2\lambda_1^2+1\right)\left(\beta_{n_1}^2\lambda_2^2+1\right)} \cdot\left[L_1\delta_{mm_1} + \frac{\lambda_1}{\alpha_m^2\lambda_1^2+1}\left(1+(-1)^{m+m_1}\right) \cdot\left((-1)^m e^{-L_1/\lambda_1} - 1\right)\right]\left[L_2(\delta_{nn_1}+\delta_{n0}\delta_{n_10}) + \frac{\lambda_2}{\beta_n^2\lambda_2^2+1}\left(1+(-1)^{n+n_1}\right)\left((-1)^n e^{-L_2/\lambda_2} - 1\right)\right], \tag{C7}$$

$$Q^{kmn}_{m_1n_1} = \int_\Omega R_{m_1n_1}(\mathbf{x})\cos(\alpha_k x_1)\cos(\alpha_m x_1)\cos(\beta_n x_2)d\mathbf{x} = \frac{\lambda_1\lambda_2\sigma_Y^2}{2\left(\alpha_{m_1}^2\lambda_1^2+1\right)\left(\beta_{n_1}^2\lambda_2^2+1\right)} \cdot\left[L_1\left(\delta_{m_1,m+k}+\delta_{m,m_1+k}+\delta_{k,m+m_1}\right) + \lambda_1\left(\eta^-_{mk}+\eta^+_{mk}\right)\left(1+(-1)^{m+m_1}\right)\left((-1)^m e^{-L_1/\lambda_1}-1\right)\right] \cdot\left[L_2(\delta_{nn_1}+\delta_{n0}\delta_{n_10}) + \frac{\lambda_2}{\beta_n^2\lambda_2^2+1}\left(1+(-1)^{n+n_1}\right) \cdot\left((-1)^n e^{-L_2/\lambda_2}-1\right)\right], \tag{C8}$$

and $\eta^-_{mk} = [(\alpha_m - \alpha_k)^2\lambda_1^2 + 1]^{-1}$, $\eta^+_{mk} = [(\alpha_m + \alpha_k)^2\lambda_1^2 + 1]^{-1}$.

[37] Similarly, the cross covariance $C_{Yh}(\mathbf{x}'; \mathbf{y}, \tau) = \langle Y'(\mathbf{x})h^{(1)}(\mathbf{y}, \tau)\rangle$ can be derived as

$$C_{Yh}(\mathbf{x};\mathbf{y},\tau) = \frac{4}{D}\sum_{\substack{m=1\\ n=0}}^{\infty}\frac{a_n\alpha_m\sin(\alpha_m y_1)\cos(\beta_n y_2)}{\alpha_m^2+\beta_n^2}R_{mn}(\mathbf{x})J_{mn}(\tau) - \frac{8T_G}{DL_1S}\sum_{\substack{m,k=1\\ n=0}}^{\infty}a_n b_k P_{kmn}(\tau)\alpha_m\sin(\alpha_m y_1)\cos(\beta_n y_2) \cdot R_{kmn}(\mathbf{x}), \tag{C9}$$

where

$$R_{kmn}(\mathbf{x}) = \int_\Omega C_Y(\mathbf{x}',\mathbf{x})\cos\left(\alpha_m x_1'\right)\cos\left(\alpha_k x_1'\right)\cos\left(\beta_n x_2'\right)d\mathbf{x}' = \frac{\lambda_1\lambda_2\sigma_Y^2}{2\left(\beta_n^2\lambda_2^2+1\right)} \cdot\left\{2\,\eta^+_{mk}\cos[(\alpha_m+\alpha_k)x_1] + 2\,\eta^-_{mk}\cos[(\alpha_m-\alpha_k)x_1] - \left(\eta^+_{mk}+\eta^-_{mk}\right)\left[e^{-x_1/\lambda_1} + (-1)^m e^{(x_1-L_1)/\lambda_1}\right]\right\} \times\left[2\cos(\beta_n x_2) - e^{-x_2/\lambda_2} - (-1)^n e^{(x_2-L_2)/\lambda_2}\right]. \tag{C10}$$

After substituting $C_{H_0h}(\mathbf{x}; \mathbf{y}, \tau)$ and $C_{Yh}(\mathbf{x}; \mathbf{y}, \tau)$ into (C1) and carrying out integrations gives

$$C_h(\mathbf{x},t;\mathbf{y},\tau) = \frac{16}{D^2}\sum_{\substack{m,m_1=1\\ n,n_1=0}}^{\infty}\frac{a_n a_{n_1}\alpha_m\alpha_{m_1}Q^{m_1n_1}_{mn}SC}{\left(\alpha_m^2+\beta_n^2\right)\left(\alpha_{m_1}^2+\beta_{n_1}^2\right)}J_{mn}(t)J_{m_1n_1}(\tau) - \frac{32T_G}{D^2L_1S}\sum_{\substack{m,m_1,k_1=1\\ n,n_1=0}}^{\infty} \cdot\frac{a_n a_{n_1}\alpha_m\alpha_{m_1}b_{k_1}P_{k_1m_1n_1}(\tau)\,SC}{\alpha_m^2+\beta_n^2}Q^{k_1m_1n_1}_{mn}J_{mn}(t) - \frac{32T_G}{D^2L_1S}\sum_{\substack{m,m_1,k=1\\ n,n_1=0}}^{\infty}\frac{a_n a_{n_1}\alpha_m\alpha_{m_1}b_k P_{kmn}(t)SC}{\alpha_{m_1}^2+\beta_{n_1}^2} \cdot Q^{kmn}_{m_1n_1}J_{m_1n_1}(\tau) + \frac{64T_G^2}{D^2L_1^2S^2}\sum_{\substack{m,m_1,k,k_1=1\\ n,n_1=0}}^{\infty} \cdot a_n a_{n_1}\alpha_m\alpha_{m_1}b_k b_{k_1}P_{kmn}(t)P_{k_1m_1n_1}(\tau)SC\,Q^{k_1m_1n_1}_{kmn}, \tag{C11}$$

where

$$Q^{k_1m_1n_1}_{kmn} = \int_\Omega R_{kmn}(\mathbf{x})\cos(\alpha_{k_1}x_1)\cos(\alpha_{m_1}x_1)\cos\left(\beta_{n_1}x_2\right)d\mathbf{x} = \frac{\lambda_1\lambda_2\sigma_Y^2}{4\left(\beta_n^2\lambda_2^2+1\right)}\left[L_1\eta^+_{mk}\left(\delta_{m+k,m_1+k_1}+\delta_{k_1,m+k+m_1} + \delta_{m_1,m+k+k_1}\right) + L_1\eta^-_{mk}\left(\delta_{k,m+m_1+k_1}+\delta_{m,k+m_1+k_1} + \delta_{m+m_1,k+k_1}+\delta_{m+k_1,m_1+k}\right) + \lambda_1\left(\eta^-_{mk}+\eta^+_{mk}\right) \cdot\left(\eta^-_{m_1k_1}+\eta^+_{m_1k_1}\right)\left(1+(-1)^{m+k}\right) \cdot\left((-1)^{m_1+k_1}e^{-L_1/\lambda_1}-1\right)\right]\left[L_2(\delta_{nn_1}+\delta_{n0}\delta_{n_10}) + \frac{\lambda_2}{\beta_{n_1}^2\lambda_2^2+1}\left(1+(-1)^{n+n_1}\right)\left((-1)^{n_1}e^{-L_2/\lambda_2}-1\right)\right]. \tag{C12}$$

In particular, letting $t = \infty$ and $\tau = \infty$, we obtain the steady state head variance

$$C_h(\mathbf{x};\mathbf{y}) = \frac{16J_1^2}{D^2} \sum_{\substack{m,m_1=1 \\ n,n_1=0}}^{\infty} \frac{a_n a_{n_1} \alpha_m \alpha_{m_1} Q_{mn}^{m_1 n_1} SC}{\left(\alpha_m^2 + \beta_n^2\right)\left(\alpha_{m_1}^2 + \beta_{n_1}^2\right)}. \tag{C13}$$

[38] **Acknowledgments.** This work was supported by DOE/NGOTP under contract AC1005000. We thank two anonymous reviewers and the Associate Editor for their helpful comments and suggestions for improving the paper.

References

Ballio, F., and A. Guadagnini (2004), Convergence assessment of numerical Monte Carlo simulations in groundwater hydrology, *Water Resour. Res.*, *40*, W04603, doi:10.1029/2003WR002876.

Dagan, G. (1979), Models of groundwater flow in statistically homogeneous porous formations, *Water Resour. Res.*, *15*, 47–63.

Dagan, G. (1982), Stochastic modeling of groundwater flow by unconditional and conditional probabilities: 1. Conditional simulation and the direct problem, *Water Resour. Res.*, *18*, 813–833.

Dagan, G. (1985), Stochastic modeling of groundwater flow by unconditional and conditional probabilities: The inverse problem, *Water Resour. Res.*, *21*, 65–72.

Dagan, G. (1989), *Flow and Transport in Porous Formations*, Springer, New York.

Dettinger, M. D., and J. Wilson (1981), First-order analysis of uncertainty in numerical models of groundwater flow: 1. Mathematical development, *Water Resour. Res.*, *17*, 149–161.

Freeze, R. A. (1975), A stochastic-conceptual analysis of one-dimensional groundwater flow in nonuniform homogeneous media, *Water Resour. Res.*, *11*, 725–741.

Gelhar, L. W. (1993), *Stochastic Subsurface Hydrology*, Prentice-Hall, Upper Saddle River, N. J.

Gelhar, L. W., and C. L. Axness (1983), Three-dimensional stochastic analysis of macrodispersion in aquifers, *Water Resour. Res.*, *19*, 161–180.

Guadagnini, A., and S. P. Neuman (1999a), Nonlocal and localized analyses of conditional mean steady state flow in bounded, randomly nonuniform domains: 1. Theory and computational approach, *Water Resour. Res.*, *35*, 2999–3018.

Guadagnini, A., and S. P. Neuman (1999b), Nonlocal and localized analyses of conditional mean steady state flow in bounded, randomly nonuniform domains: 2. Computational examples, *Water Resour. Res.*, *35*, 3019–3039.

Guadagnini, A., M. Riva, and S. P. Neuman (2003), Three-dimensional steady state flow to a well in a randomly heterogeneous bounded aquifer, *Water Resour. Res.*, *39*(3), 1048, doi:10.1029/2002WR001443.

Gutjahr, A. L., and L. W. Gelhar (1981), Stochastic models of subsurface flow: Infinite versus finite domains and stationarity, *Water Resour. Res.*, *17*, 337–350.

Mizell, S. A., A. L. Gutjahr, and L. W. Gelhar (1982), Stochastic analysis of spatial variability in two-dimensional steady groundwater flow assuming stationary and nonstationary heads, *Water Resour. Res.*, *18*, 1053–1067.

Neuman, S. P., and S. Orr (1993), Prediction of steady state flow in nonuniform geologic media by conditional moments: Exact nonlocal formalism, effective conductivities, and weak approximation, *Water Resour. Res.*, *29*, 341–364.

Osnes, H. (1995), Stochastic analysis of head spatial variability in bounded rectangular heterogeneous aquifers, *Water Resour. Res.*, *31*, 2981–2990.

Osnes, H. (1998), Stochastic analysis of velocity spatial variability in bounded rectangular heterogeneous aquifers, *Adv. Water Resour.*, *21*, 203–215.

Özişik, M. N. (1989), *Boundary Value Problems of Heat Conduction*, Dover, Mineola, N. Y.

Riva, M., A. Guadagnini, S. P. Neuman, and S. Franzetti (2001), Radial flow in a bounded, randomly heterogeneous aquifer, *Transp. Porous Media*, *45*, 139–193.

Rubin, Y., and G. Dagan (1988), Stochastic analysis of boundary effects on head spatial variability in heterogeneous aquifers: 1. Constant head boundary, *Water Resour. Res.*, *24*, 1689–1697.

Rubin, Y., and G. Dagan (1989), Stochastic analysis of boundary effects on head spatial variability in heterogeneous aquifers: 2. Impervious boundary, *Water Resour. Res.*, *25*, 707–712.

Rubin, Y., and G. Dagan (1992), A note on head and velocity covariances in three-dimensional flow through heterogeneous anisotropic porous media, *Water Resour. Res.*, *28*, 1463–1470.

Smith, L., and R. A. Freeze (1979), Stochastic analysis of steady state groundwater flow in a bounded domain: 2. Two-dimensional simulations, *Water Resour. Res.*, *15*, 1543–1559.

Tartakovsky, D. M., and S. P. Neuman (1998), Transient flow in bounded randomly heterogeneous domains: 1. Exact conditional moment equations and recursive approximations, *Water Resour. Res.*, *34*, 1–12.

Zhang, D. (1999), Quantification of uncertainty for fluid flow in heterogeneous petroleum reservoirs, *Phys. D*, *133*, 488–497.

Zhang, D. (2002), *Stochastic Methods for Flow in Porous Media*, Elsevier, New York.

Zhang, D., and Z. Lu (2004), An efficient, higher-order perturbation approach for flow in randomly heterogeneous porous media via Karhunen-Loeve decomposition, *J. Comput. Phys.*, *194*, 773–794.

Zhang, D., and S. P. Neuman (1992), Comment on "A note on head and velocity covariances in three-dimensional flow through heterogeneous anisotropic porous media" by Y. Yubin and G. Dagan, *Water Resour. Res.*, *28*, 3345–3346.

Zyvoloski, G. A., B. A. Robinson, Z. V. Dash, and L. L. Trease (1997), Summary of the models and methods for the FEHM application—A Finite-Element Heat- and Mass-Transfer code, *Rep. LA-13307-MS*, Los Alamos Natl. Lab., Los Alamos, N. M.

Z. Lu, Hydrology, Geochemistry, and Geology Group (EES-6), MS T003, Los Alamos National Laboratory, Los Alamos, NM 87545, USA. (zhiming@lanl.gov)

D. Zhang, Mewbourne School of Petroleum and Geological Engineering, University of Oklahoma, 100 East Boyd, SEC T301, Norman, OK 73019, USA. (donzhang@ou.edu)